

Sector of the 2^{++} mesons: observation of the tensor glueball

V.V. Anisovich^a, M.A. Matveev^a, J. Nyiri^b and A.V. Sarantsev^{a,c}

^a Petersburg Nuclear Physics Institute, Gatchina 188300, Russia

^b KFKI Research Institute for Particle
and Nuclear Physics, Budapest, Hungary

^c HISKP, Universität Bonn, D-53115 Germany

17.03.05

Abstract

Data of the Crystal Barrel and L3 collaborations clarified essentially the situation in the 2^{++} sector in the mass region up to 2400 MeV, demonstrating the linearity of (n, M^2) trajectories, where n is the radial quantum number of a quark-antiquark state with mass M . We discuss these data and show that there exists a superfluous state for the (n, M^2) trajectories: a broad resonance $f_2(2000)$. We pay special attention to the reactions $p\bar{p} \rightarrow \pi\pi, \eta\eta, \eta\eta'$ in the mass region 1990–2400 MeV where, together with $f_2(2000)$, four relatively narrow resonances are seen: $f_2(1920)$, $f_2(2020)$, $f_2(2240)$, $f_2(2300)$. We analyse the branching ratios of all these resonances and show that only the decay couplings of the broad state $f_2(2000) \rightarrow \pi^0\pi^0, \eta\eta, \eta\eta'$ satisfy relations inherent in the glueball decay.

PACS numbers: 14.40-n, 12.38-t, 12.39-MK

1 Introduction

A broad isoscalar-tensor resonance in the region of 2000 MeV is seen in various reactions [1]. Recent measurements give:

$M = 2010 \pm 25$ MeV, $\Gamma = 495 \pm 35$ MeV in $p\bar{p} \rightarrow \pi^0\pi^0, \eta\eta, \eta\eta'$ [2],

$M = 1980 \pm 20$ MeV, $\Gamma = 520 \pm 50$ MeV in $pp \rightarrow pp\pi\pi\pi\pi$ [3],

$M = 2050 \pm 30$ MeV, $\Gamma = 570 \pm 70$ MeV in $\pi^- p \rightarrow \phi\phi n$ [4];

following them, we denote the broad resonance as $f_2(2000)$.

The large width of $f_2(2000)$ arouses the suspicion that this state is a tensor glueball. Such an opinion was expressed lately in different publications.

In [5], Chapter 5.4, it is said that the very broad isoscalar 2^{++} state observed in the region ~ 2000 MeV with a width of the order of $400 - 500$ MeV [3] could well be the trace of a tensor glueball lying on the Pomeron trajectory.

Another argument comes from the analysis of the mass shifts of the $q\bar{q}$ tensor mesons ([6], Section 12). It is stated here that the mass shift between $f_2(1560)$ and $a_2(1700)$ can not be explained by the mixing of non-strange and strange components in the isoscalar sector: in such a mixing the average mass squared does not change and we should find $f_2(1750)$ at a much higher mass. Instead, we observe a shift down in masses of both isoscalar states. Such a phenomenon can be an indication for the presence of a tensor glueball in the mass region $1800-2000$ MeV.

In [4], the following argument is presented: a significant violation of the OZI-rule in the production of tensor mesons with dominant $s\bar{s}$ components (reactions $\pi^-p \rightarrow f_2(2120)n$, $f_2(2340)n$, $f_2(2410)n \rightarrow \phi\phi n$ [7]) is due to the presence of a broad glueball state $f_2(2000)$ in this region, resulting in a noticeable admixture of the glueball component in $f_2(2120)$, $f_2(2340)$, $f_2(2410)$.

The possibility that the broad resonance $f_2(2000)$ could be a glueball is discussed also in [8], Section 10. Here, however, a problem in the identification of $f_2(2000)$ as the tensor glueball is stressed. As it is written in Subsection 10.6, of [8] the prediction for the branching fraction of the 2^+ glueball is large if the width is taken to be the 500 MeV fitted to $f_2(1950)$. Observed decays to $\sigma\sigma$ and $f_2(1270)\sigma$ account for $(10 \pm 0.7 \pm 3.6) \cdot 10^{-4}$ of J/Ψ radiative decays and for a further $(7 \pm 1 \pm 2) \cdot 10^{-4}$ in $K^*\bar{K}^*$ decays. If one assumes flavour-blindness for vector-vector final states, the vector-vector contribution increases to $(16 \pm 2 \pm 4.5) \cdot 10^{-4}$. The total $2.6 \cdot 10^{-3}$ is still less by a factor 9 than predicted for a glueball; in [8] this is considered as a problem in identifying $f_2(1950)$ with the 2^+ glueball.

In [9] it was emphasised that the $f_2(2000)$ being superfluous for $q\bar{q}$ systematics can be considered as the lowest tensor glueball. A recent re-analysis of the $\phi\phi$ spectra [4] in the reaction $\pi^-p \rightarrow \phi\phi n$ [7], the study of the processes $\gamma\gamma \rightarrow \pi^+\pi^-\pi^0$ [10], $\gamma\gamma \rightarrow K_S K_S$ [6] and the analysis of the $p\bar{p}$ annihilation in flight $p\bar{p} \rightarrow \pi\pi, \eta\eta, \eta\eta'$ [2] clarified essentially the status of the ($J^{PC} = 2^{++}$)-mesons. This allows us to place the f_2 mesons reliably on the (n, M^2) -trajectories [9], where n is the radial quantum number of the $q\bar{q}$ -state. In the present review we discuss the data for $\gamma\gamma \rightarrow \pi^+\pi^-\pi^0$ [10], $\gamma\gamma \rightarrow K_S K_S$ [6] and $p\bar{p} \rightarrow \pi\pi, \eta\eta, \eta\eta'$ [2] in Section 2.

In [11] (see also [5, 12]), the known $q\bar{q}$ -mesons consisting of light quarks ($q = u, d, s$) are placed on the (n, M^2) trajectories. Trajectories for mesons with various quantum numbers turn out to be linear with a good accuracy. In Section 3 we give a systematisation of tensor mesons, f_2 and a_2 , on the (n, M^2) planes.

The quark states with ($I = 0$, $J^{PC} = 2^{++}$) are determined by two flavour components $n\bar{n} = (u\bar{u} + d\bar{d})/\sqrt{2}$ and $s\bar{s}$ for which two states ${}^{2S+1}L_J = {}^3P_2, {}^3F_2$ are possible. Consequently, we have four trajectories on the (n, M^2) plane. Generally speaking, the f_2 -states are mixtures of both the flavour components and the $L = 1, 3$ waves. The real situation is, however, such that the lowest trajectory [$f_2(1275)$, $f_2(1580)$, $f_2(1920)$, $f_2(2240)$] consists of mesons with dominant ${}^3P_2 n\bar{n}$ components, while the trajectory [$f_2(1525)$, $f_2(1755)$, $f_2(2120)$, $f_2(2410)$] contains mesons with predominantly ${}^3P_2 s\bar{s}$ components. The F -trajectories are presently represented

by three resonances [$f_2(2020)$, $f_2(2300)$] and [$f_2(2340)$] with the corresponding dominant $^3F_2 n\bar{n}$ and $^3F_2 s\bar{s}$ states. In [9], it is shown that the broad resonance $f_2(2000)$ is not part of those states placed on the (n, M^2) trajectories. In the region of 2000 MeV three $n\bar{n}$ -dominant resonances, $f_2(1920)$, $f_2(2000)$ and $f_2(2020)$, are seen, while on the (n, M^2) -trajectories there are only two vacant places. This means that one state is obviously superfluous from the point of view of the $q\bar{q}$ -systematics, i.e. it has to be considered as exotics.

There exist various arguments in favour of the assumption that $f_2(2000)$ is generated by a glueball. Still, it can not be a pure gluonic $f_2(2000)$ state: it follows from the $1/N$ expansion rules [33, 34] that the gluonic state ($q\bar{q}$) mixes with quarkonium systems (gg) without suppression. The problem of the mixing of (gg) and ($q\bar{q}$) systems is discussed in Section 4, where we present also the relations between decay constants of a glueball into two pseudoscalar mesons $glueball \rightarrow PP$ and into two vector mesons $glueball \rightarrow VV$.

In Section 5 we demonstrate that just $f_2(2000)$ is the glueball.

In [13] it was pointed out that an exotic state has to be broad. Indeed, if an exotic resonance occurs among the standard $q\bar{q}$ -states, they overlap, and their mixing becomes possible due to large distance transition: the *resonance*(1) \rightarrow *real mesons* \rightarrow *resonance*(2). Owing to these transitions, an exotic meson accumulates the widths of its neighbouring resonances. The phenomenon of the accumulation of widths was studied in the scalar sector near 1500 MeV [14, 15]. In [15], a model of mixing of the gluonium gg with the neighbouring quarkonium states was considered. It was demonstrated that, as a result of mixing, it is precisely the gluonium state which transforms into a broad resonance. The reason is that $q\bar{q}$ states being orthogonal to each other mix weakly, while the gluonium mixes with neighbouring $q\bar{q}$ states without suppression. Therefore, the gluonium "dives" more rapidly into the complex M -plane. The mixing of states is always accompanied by a repulsion of the corresponding poles: when poles are in the complex M -plane at approximately the same $\text{Re } M$, this repulsion results in "sinking" one of them into the region of large and negative $\text{Im } M$ and "pulling" others to the real M -axis.

Hence, the large width of $f_2(2000)$ can indicate that this state is an exotic one. Strictly speaking, this fact is not sufficient to prove that $f_2(2000)$ is a glueball. At the moment a variety of versions for exotic mesons is discussed; these are $q\bar{q}g$ hybrids as well as multiquark states (see, e.g. [5, 8, 12] and references therein). Thus, in order to fix $f_2(2000)$ as a glueball, it is of great importance to investigate the decay couplings and prove that they satisfy relations characterising the glueball. The coupling constants for the transitions

$$f_2(1920), f_2(2000), f_2(2020), f_2(2240), f_2(2300) \rightarrow \pi\pi, \eta\eta, \eta\eta'$$

are separated in [16, 17] on the basis of a partial wave analysis [2] carried out earlier. The coupling constants obtained in [16, 17] indicate that only the decays $f_2(2000) \rightarrow \pi^0\pi^0, \eta\eta, \eta\eta'$ obey the relations corresponding to a glueball, while the decay constants for other resonances do not fulfil such conditions. Note that the glueball decay couplings are close to those for the $SU(3)$ -flavour singlet, but, because of the flavour symmetry violation caused by the strange quark, do not coincide with them exactly.

Let us remind that there are two more arguments in favour of the glueball nature of $f_2(2000)$:

- (i) the Pomeron trajectory, determined on the basis of data on high-energy hadron decays (see, e.g., [18, 19, 20]), indicates that a tensor glueball has to have a mass of the order of $1.7\text{--}2.3\text{ GeV}$;
- (ii) lattice calculations [21] lead to a similar value, $M_{2+-\text{glueball}} \sim 2.3\text{--}2.5\text{ GeV}$.

We have one, sufficiently general, argument against the interpretation of $f_2(2000)$ as an exotic $q\bar{q}g$ or $qq\bar{q}\bar{q}$ state: the absence of any serious facts confirming their existence. Indeed, if such states existed, we would see a large number of them in the mass region above 1500 MeV. Moreover, we could observe not only exotic states; the number of resonances with "normal" quantum numbers would also be seriously increased. However, the systematics of quarks on the (n, M^2) -plane does not reveal such an increase: almost all observed resonances can be interpreted as $q\bar{q}$ states (see [5], Chapter 5). Apparently, Nature does not like coloured multiparticle objects. The same conclusion follows from the systematisation of baryons: experimental data give a much smaller amount of excited states, than calculations in the framework of a three-quark model [22] do. One gets the impression that excited baryons are rather quark-diquark systems (see discussions in [5, 23].

Owing to the $1/N$ expansion rules, the gluonium component is relatively small in the quark state f_2 : its probability is suppressed as $1/N_c$. In Section 6 we determine the mixing angle of the $n\bar{n}$ and $s\bar{s}$ components in the quark f_2 -mesons, making use of the relations between the decay constants $f_2 \rightarrow \pi\pi, \eta\eta, \eta\eta'$. Also, we estimate the possible changes in the mixing angle as a consequence of a gluonium component in the quark state f_2 .

In the Conclusion, we discuss the situation in the glueball sector.

Up to now, two glueball states, the scalar meson $f_0(1200\text{--}1600)$ and the tensor $f_2(2000)$ are observed. Both states are broad ones, and the coupling constants corresponding to their decays into pseudoscalar mesons (channels $\text{glueball} \rightarrow PP$) satisfy just the relations characterising the glueball. The next states which are of interest are radial excitations of the scalar and tensor gluonia, and the pseudoscalar glueball. Taking the Pomeron trajectories on the (J, M^2) -plane as a basis, we predict the masses of excited scalar and tensor glueball states.

2 Analysis of the data for tensor mesons

We demonstrate here the results obtained from the data analysis used in performing the systematisation of the f_2 resonances and extracting the decay couplings $f_2 \rightarrow \pi\pi, \eta\eta, \eta\eta'$.

2.1 L3 data on the $\gamma\gamma \rightarrow \pi^+\pi^-\pi^0$ reaction

In this reaction the $\gamma\gamma$ channel couples only to states with $C=+1$ parity; 3π has a negative G-parity. For a $q\bar{q}$ system one has $G = Ce^{i\pi I}$, so the $I = 1$ quark-antiquark states are produced only in the $\gamma\gamma$ channel. Due to C -parity conservation in neutral decay modes, only f -states with $(J^{PC} = 0^{++}, 2^{++}, 4^{++} \dots)$ are produced in the $\pi^+\pi^-$ channel. In the $\pi^\pm\pi^0$ channel only isovector mesons with $J^{PC} = 1^{--}, 3^{--} \dots$ are produced.

The $\gamma\gamma$ mass distribution is dominated by the production of the $a_2(1320)$ resonance, see

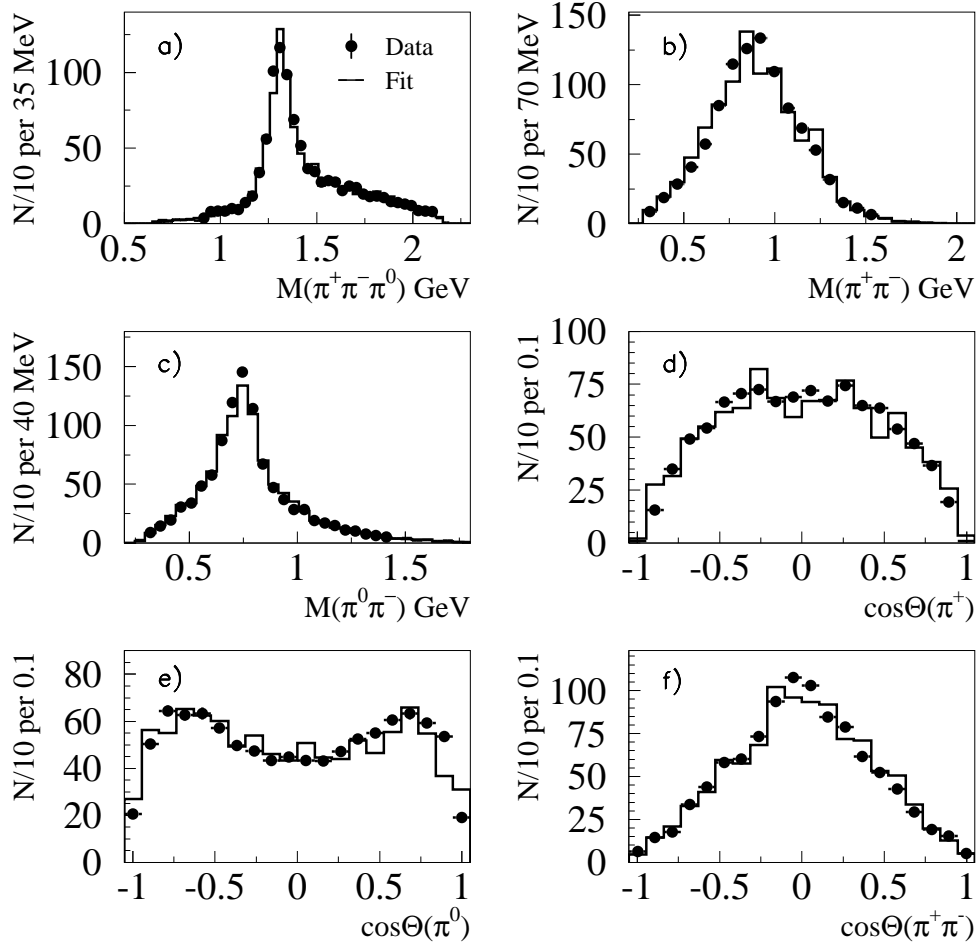


Figure 1: Reaction $\gamma\gamma \rightarrow \pi^+\pi^-\pi^0$. a) $\gamma\gamma$ mass spectrum, b,c) $\pi^+\pi^-$ and $\pi^\pm\pi^0$ mass spectra, d,e) the angular distributions of charged and neutral pions in the c.m.s. of the reaction, f) the angular distribution between charged and neutral pion in the c.m.s. of two charged pions.

Fig. 1a. One can see a prominent structure in the mass region 1.6-1.8 GeV as well as a possible contribution at the $a_2(1320)$ signal.

The $\pi^+\pi^-$ mass distribution is shown in Fig. 1b. There are no clear signals in the data coming from well known narrow scalar-isoscalar states $f_0(980)$ and $f_0(1500)$. Indeed, the partial wave analysis shows very small contributions of these mesons; such decay modes were omitted in the final fit.

A signal coming from $f_2(1275)\pi^0$ is observed at high $\gamma\gamma$ energies; this is important to describe the two-pion mass spectrum and angular distributions.

The $\pi\pi \rightarrow \pi\pi$ S-wave amplitude has a broad component which covers the mass region from the $\pi\pi$ threshold up to 2 GeV. Such a component is introduced in the present analysis and is

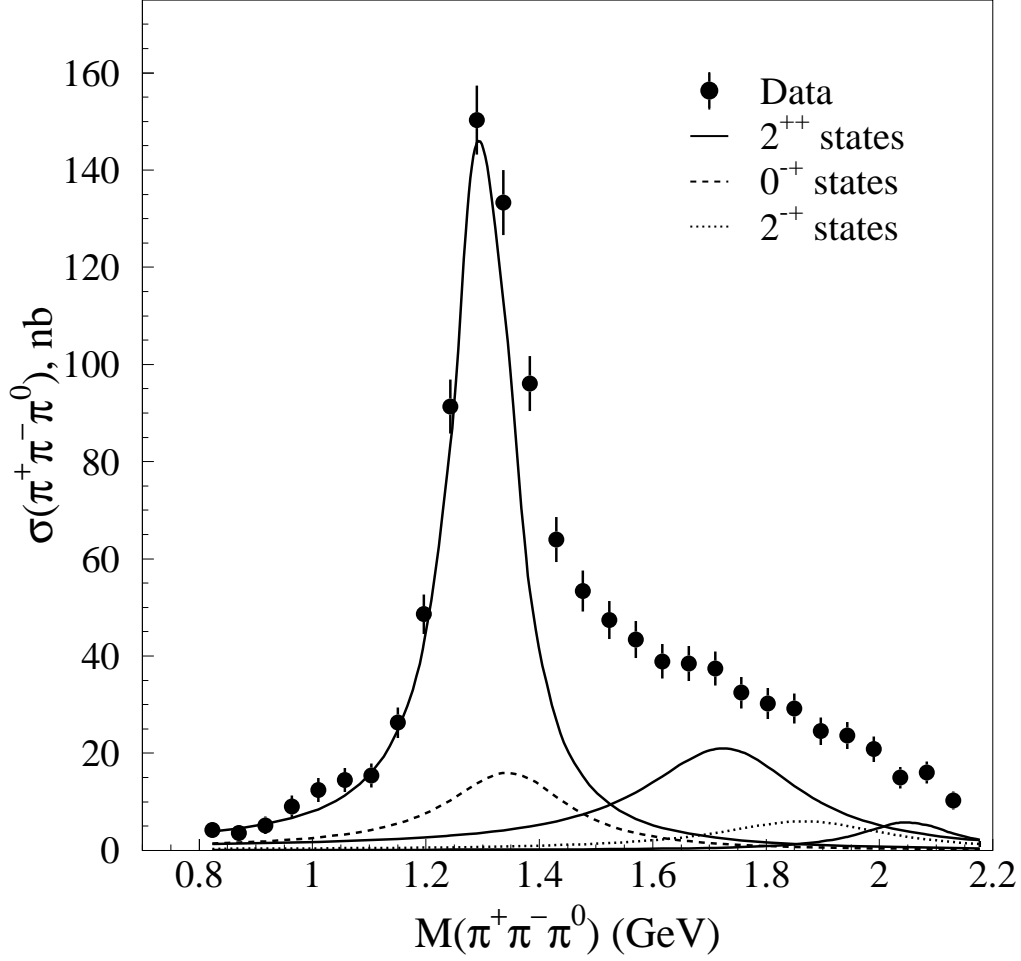


Figure 2: Reaction $\gamma\gamma \rightarrow \pi^+\pi^-\pi^0$. The contribution of different resonances listed in Table 1 to the cross section: full curves - 2^{++} states, dashed curves - 0^{-+} states and dotted curves - the contribution of 2^{-+} states.

parametrized in two different ways.

The first parametrisation is taken from [24]. It was introduced to describe the CERN-Munich data on $(\pi^-p \rightarrow \pi^+\pi^-n)$ [25] and the Crystal Barrel data on proton-antiproton annihilation into $3\pi^0$ and $2\eta\pi^0$ channels simultaneously. To simulate a possible s -dependence of the vertex (which can be important for this very broad state), we use the method suggested in [24].

The second parametrisation was used in [26]. It covers the mass region up to 1.9 GeV and describes, in the framework of the P-vector/K-matrix approach, a much larger number of two- and three-body reactions. To avoid an over-parametrisation of the fit, we vary only the production couplings of the two lowest K-matrix poles.

The main signal in the $\pi^\pm\pi^0$ mass spectrum is due to the production of $\rho(770)$. There is

very little structure in the region higher than 1 GeV (see Fig. 1c) and the signal is almost zero at masses above 1.5 GeV. Because of this, neither $\rho_3(1690)$, nor $\rho(1770)$ has to be introduced in the analysis. A contribution from $\rho(1450)$ is found to be useful to describe the data: however, this state is quite broad and possibly simulates a non-resonant two pion production in this channel.

In the $\pi^+\pi^-\pi^0$ spectrum one can see a strong signal coming from $a_2(1320)$; the characteristics of this resonance were defined with high precision by the VES collaboration [27]. It is not surprising that the $\gamma\gamma \rightarrow 3\pi$ data are dominated by the production of the $a_2(1320)$ state, since this resonance has the highest spin in the mass region below 1.6 GeV (the $\gamma\gamma$ cross section is proportional to $(2J+1)$) and it is a ground $q\bar{q}$ state with the radial quantum number $n=1$. Indeed, the $\gamma\gamma \rightarrow \text{resonance}$ production amplitude is a convolution of the photon and the quark-antiquark resonance wave functions [28, 29, 30]. This provides a suppression of nearly an order for the production of the radially excited states ($n \geq 2$) [29]. Nevertheless, there is a manifest contribution of the higher tensor state. While $a_2(1320)$ decays practically only into the $\rho(770)\pi$ channel, the second tensor state decays almost equally to $\rho(770)\pi$ and $f_2(1275)\pi$. This fact allows us to identify this state with a good accuracy.

The solution reveals quite a large contribution coming from the 0^{-+} partial wave decaying into $f_0\pi$. There is, however, a problem in distinguishing it from the experimental background: such a decay, giving S-wave amplitudes in all decay channels, provides very smooth structures in mass distributions and, moreover, these amplitudes do not interfere with the tensor amplitude.

The contribution of the 2^{-+} state is found to be quite small when fitted to the $\pi_2(1670)$ state (see Table 1). If it is fitted with free Breit-Wigner parameters, it is always optimised at higher masses (~ 1870 MeV).

The $\pi^+\pi^-\pi^0$ spectrum and the contributions of resonances with different J^{PC} in the final solution are shown in Fig. 2. Masses, total widths, the $\Gamma_{\gamma\gamma}$ partial width and the branching ratio into 3π are listed in Table 1 for the considered resonances.

Table 1: Masses, total widths and the partial width $\Gamma_{\gamma\gamma \rightarrow \pi\pi\pi}$ for the resonances observed in the reaction $\gamma\gamma \rightarrow \pi^+\pi^-\pi^0$.

Resonance	M (MeV)	Γ (MeV)	$\Gamma_{\gamma\gamma}\text{Br}(3\pi)$ (keV)
$a_2(1320)$	$1302 \pm 3 \pm 6$	$118 \pm 6 \pm 10$	0.65 ± 0.05
$a_2(1730)$	$1725 \pm 25 \pm 10$	340 ± 40	$0.34^{+0.15}_{-0.06}$
$\pi(1300)$ [1]	1350 ± 40	320 ± 50	≤ 0.8
2^{-+}	1870 ± 60	325 ± 40	0.15 ± 0.03
$\pi_2(1670)$ [1]	1670	260	≤ 0.1

2.2 L3 data on the reaction $\gamma\gamma \rightarrow K_S K_S$ [6]

Important data for the identification of the tensor mesons were obtained by the L3 collaboration on the reaction $\gamma\gamma \rightarrow K_S K_S$. Only states with even spin J and positive parities $P = C = +$ contribute to two neutral pseudoscalar particles, what reduces the possible partial waves drastically. The $(2J + 1)$ factor in the cross section favours the dominant production of the tensor states. The 4^{++} states are produced at high energies ($M \geq 1.9 \text{ GeV}$).

The meson states consisting of light quarks u, d, s form meson nonets: three isospin 1, four isospin 1/2 and two isoscalar states. The isoscalar states can be a mixture of $n\bar{n} = (u\bar{u} + d\bar{d})/\sqrt{2}$ and $s\bar{s}$ components. The decay of $(I = 0)$ and $(I = 1, I_3 = 0)$ -states into two kaons is defined by the production of a new $s\bar{s}$ pair (an s -quark exchange process) and has the following structure for different isospins: $(u\bar{u} + d\bar{d})/\sqrt{2} \rightarrow K^+ K^- + K^0 \bar{K}^0$ for $I=0$, and $(u\bar{u} - d\bar{d})/\sqrt{2} \rightarrow K^+ K^- - K^0 \bar{K}^0$ for $I=1$. As a result, a strong destructive interference occurs between the $f_2(1275)$ and $a_2(1320)$ mesons which is very sensitive to the mixing angle of the isoscalar state. The flavour content of isoscalar-scalar resonances belonging to the same nonet can be written in the form

$$\begin{aligned} f_2(q\bar{q}) &= n\bar{n} \cos \varphi + s\bar{s} \sin \varphi, \\ f'_2(q\bar{q}) &= -n\bar{n} \sin \varphi + s\bar{s} \cos \varphi. \end{aligned} \quad (1)$$

Although the production of states with dominant $s\bar{s}$ components is suppressed by the smaller $\gamma\gamma$ coupling, these states usually have a larger branching ratio for the decay into the $K_S K_S$ channel, and can contribute appreciably into the total cross section.

There is no doubt about the nature of tensor resonances below 1600 MeV. The partial wave analysis showed that tensor resonances are produced dominantly in the 5S_2 $\gamma\gamma$ state, which was predicted by model calculations [29]. The model gives directly the ratio between 5S_2 and 1D_2 waves and the $\gamma\gamma$ couplings. These values can be introduced in the analysis without changing the quality of the description. The data with the lowest tensor states are shown in Fig. 3a.

We have found that the 0^{++} partial wave can be fitted well in the framework of the P-vector/K-matrix approach. The form of the 0^{++} contribution in $\gamma\gamma \rightarrow K\bar{K}$ follows closely the $\pi\pi \rightarrow K\bar{K}$ cross section, which is not surprising: the production coupling to the $s\bar{s}$ system is strongly suppressed in both reactions. The values of the coupling constants of the reactions $\gamma\gamma \rightarrow f_0, a_0$ agree well with those given in the calculations [29]: in the same way as in the tensor sector, the calculated $\gamma\gamma$ couplings can be used directly, not damaging the quality of the description.

A contribution of 4^{++} states is observed in high energy angular distributions. Some broad and some rather narrow components are seen in this wave. The broad state can be associated with $n\bar{n}$ and the narrow one with a 4^{++} $s\bar{s}$ state. The description of the data with tensor, scalar and 4^{++} states is shown in Fig. 3b.

There is a clear resonance structure in the 1750 MeV region. The angular distribution in this region follows very closely the $(1 - \cos^2 \Theta)^2$ shape which corresponds to the $^5S_2 \gamma\gamma$ production of the tensor meson. However, the acceptance decreases rapidly in the forward and backward directions providing a very similar dependence. Due to such a behaviour and to the not too

high statistics, the partial wave analysis produces almost the same angular distribution for a tensor state and for a scalar state. Still, the fit using a scalar state fails to reproduce the structure in the 1700-1800 MeV mass region. The description of the data with the best χ^2 is shown in Fig. 3c. The mass was optimised to 1805 ± 30 MeV and the width to 260 ± 30 MeV. With such a mass and width, the f_0 state can describe the slope in mass distribution above 1800 MeV. If the mass and width of the scalar state are fixed at the BES result [31] $M = 1740$ MeV, we obtain a description shown in Fig. 3d.

The main problem in a fit with a f_0 state is that there is no way to reproduce the dip in the 1700 MeV region and the slope above 1800 MeV using any (even very sophisticated) parametrisation of the resonance width. A f_0 state can interfere only with the 1D_2 component of a 2^{++} state, and this partial wave is very small in the data. Consequently, f_0 and f_2 contributions practically do not interfere and it is impossible to create a dip in the data. Contrary to this, a tensor resonance interfering with the tails of other tensor states naturally produces a dip and a good description of this mass region.

All isoscalar and isotensor states can contribute to the $\gamma\gamma \rightarrow K_S K_S$ cross section; this situation offers a very good possibility to study the reaction on the basis of the nonet classification. With $SU(3)$ relations imposed, the only parameters to fit the data for the first three states are masses, widths, the mixing angle and $SU(3)$ violation factors. We found all masses and widths for the members of the first tensor nonet to be in a very good agreement with PDG.

To describe the second nonet, we fixed parameters for $f_2(1560)$ from the Crystal Barrel results and for $a_2(1700)$ from the latest L3 analysis of the $\pi^+\pi^-\pi^0$ channel [10]. At a given mixing angle the nonet coupling was calculated to reproduce the $\pi\pi$ width of 20-25 MeV for the $f_2(1560)$ state. We found a very good description of the data with $SU(3)$ relations imposed, similar to the fit described in the previous section. The masses, widths, radii, $K\bar{K}$ couplings, mixing angles and partial widths of the states are given in Table 2; the description of the data is shown in Fig. 4.

The $f_2(1750)$ state has a mass 1755 ± 10 MeV and a total width 67 ± 12 MeV. Its $K\bar{K}$ width is 23 ± 7 MeV; the rest of the width is likely to be defined by the $K^*\bar{K}$ channel. This resonance destructively interferes with the tail of the $f'_2(1525)$ state, creating a dip in the mass region 1700 MeV. When the sign of the real part of the $f_2(1750)$ amplitude changes, this interference becomes positive, producing a clear peak in the data.

A serious problem appears in the description of the data in the framework of the nonet approach, if the peak at 1750 MeV is assumed to be owing to a scalar state. If this state is a nonet partner of one of the known states, e.g. $f_0(1370)$ or $f_0(1500)$, then the calculated signal is too weak to fit the data. If the $K\bar{K}$ coupling of this scalar state is fitted freely, we find that it must be about four times larger than the total width of the resonance. This is due to the $2J+1$ suppression factor and to the absence of a positive interference with the tail of $f'_2(1525)$ which boosts the peak in the case of a tensor state. These are problems additional to those connected with the description of the dip in the 1700 MeV region.

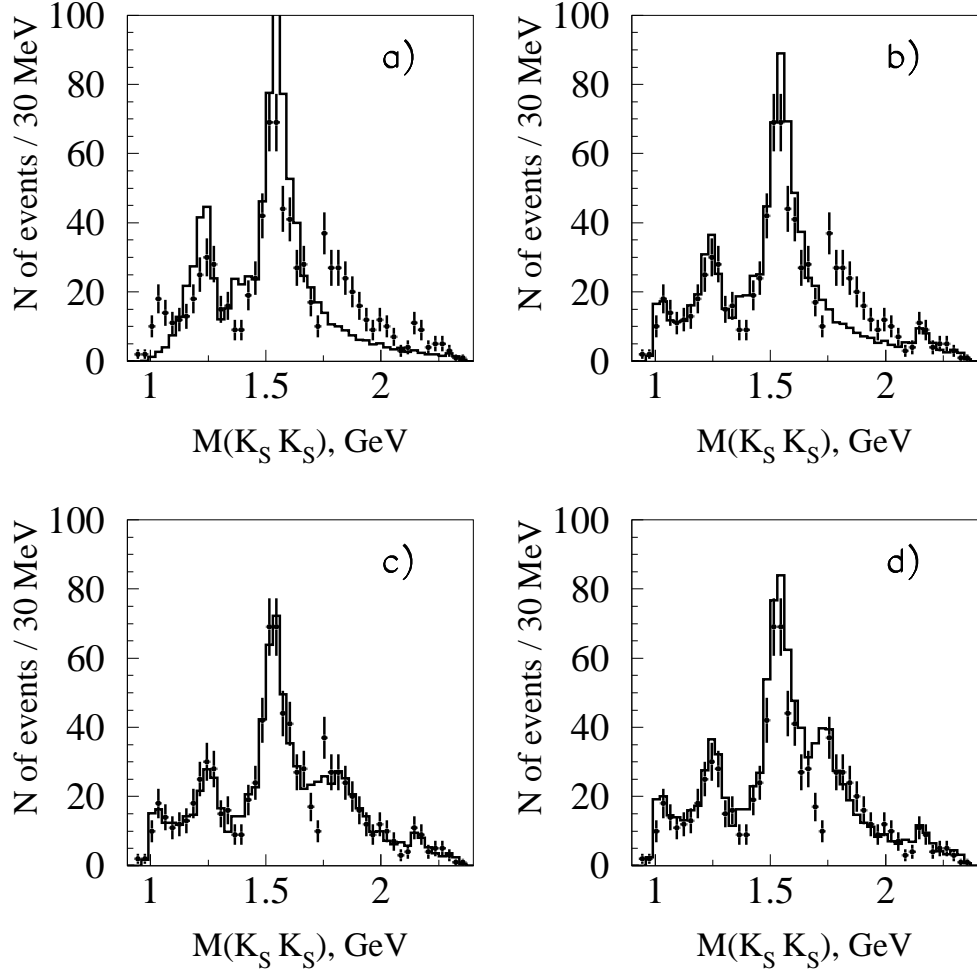


Figure 3: Reaction $\gamma\gamma \rightarrow K_S K_S$: a) the description of the data with the first tensor nonet, b) same as (a) plus scalar states and a 4^{++} state, c) same as (b) but the scalar states with free parameters, d) same as (b) but $f_0(1710)$ state with parameters fixed from the latest BES results.

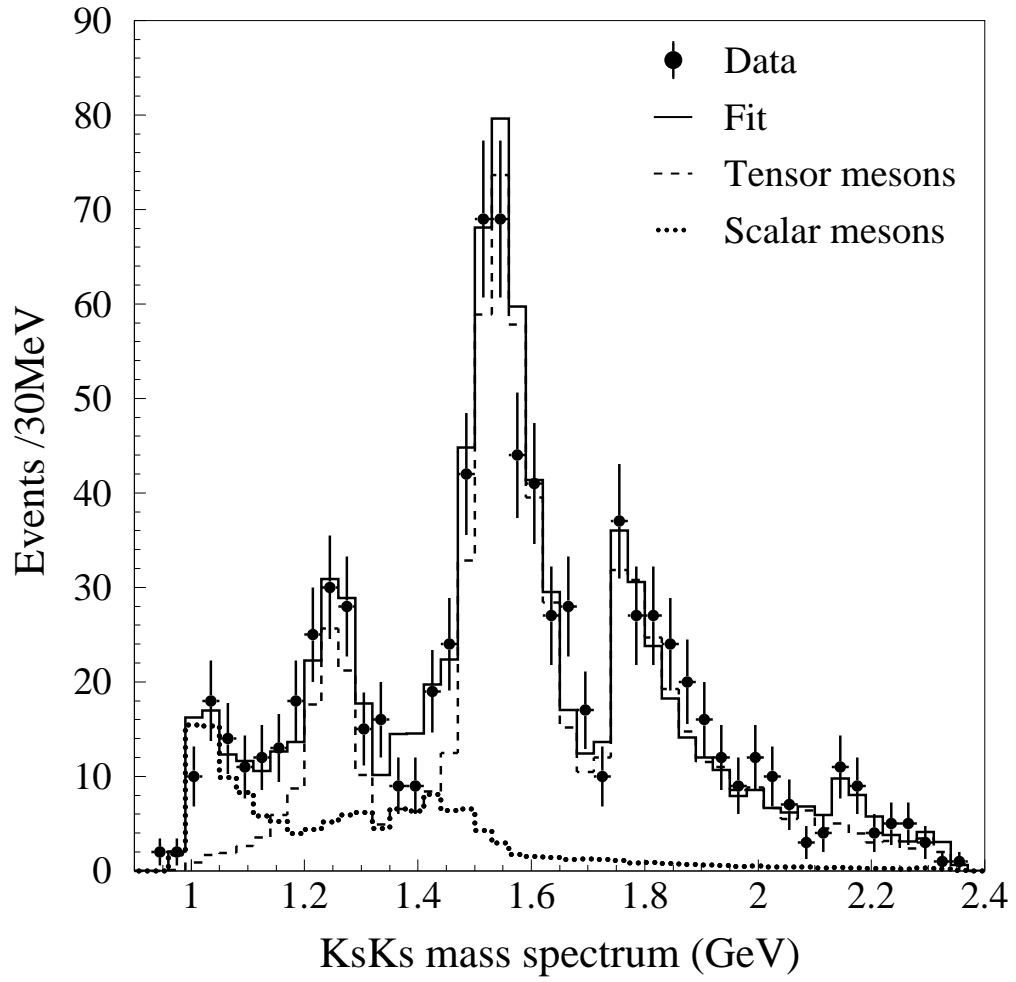


Figure 4: The description of the reaction $\gamma\gamma \rightarrow K_S K_S$ (full curve), and different contributions to the cross section: dashed curve – from the tensor states and dotted curve – from the scalar states

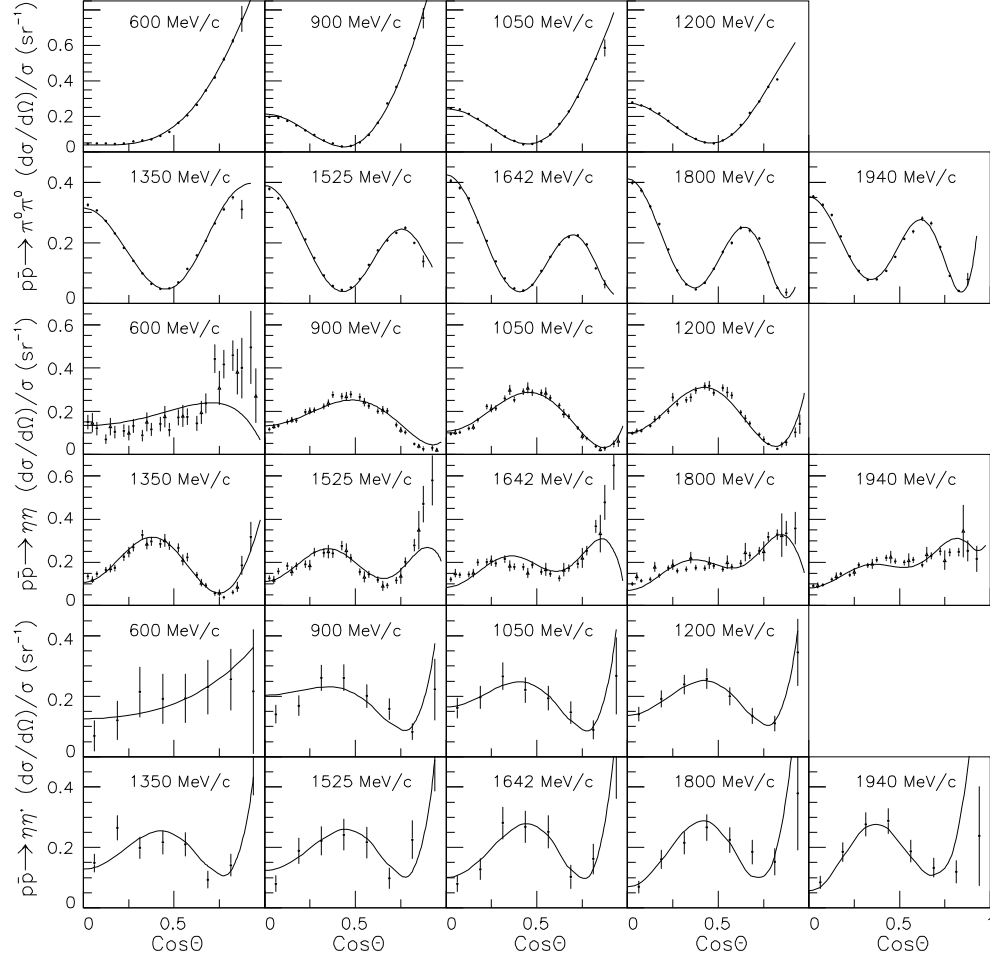


Figure 5: Angular distributions in the reactions $p\bar{p} \rightarrow \pi\pi, \eta\eta, \eta\eta'$ and their fit within resonances of Eq.(2).

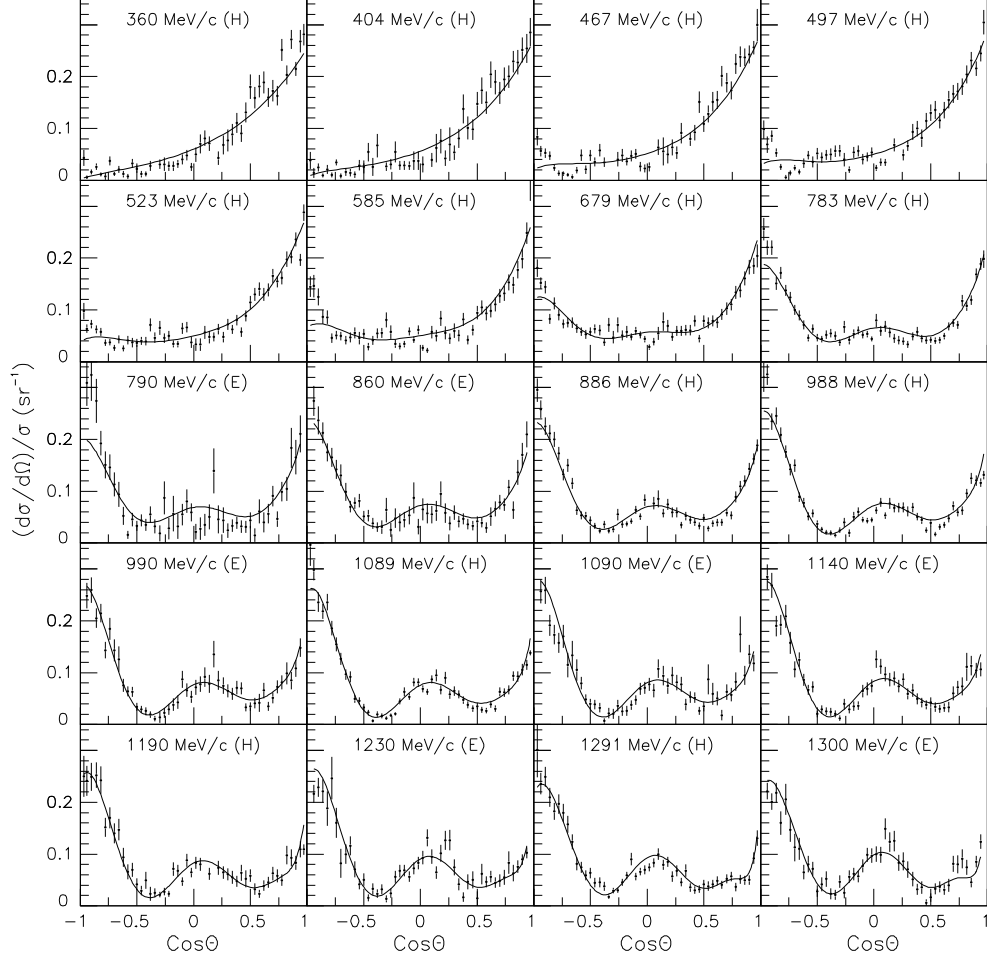


Figure 6: Differential cross sections in the reaction $p\bar{p} \rightarrow \pi^+\pi^-$ [42] at proton momenta 360-1300 MeV and their fit within resonances of Eq. (2).

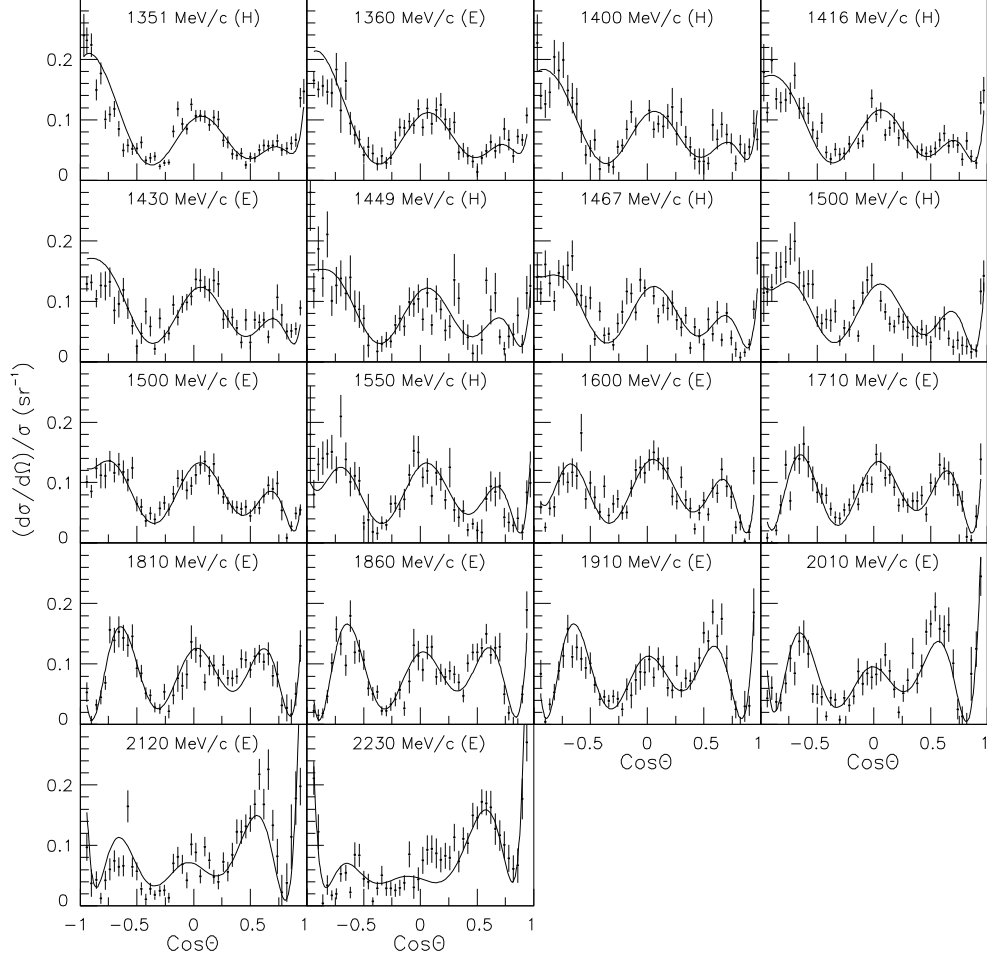


Figure 7: Differential cross sections in the reaction $p\bar{p} \rightarrow \pi^+\pi^-$ [42] at proton momenta 1350-2230 MeV and their fit within resonances of Eq.(2).

Table 2: Parameters of resonances observed in the reaction $\gamma\gamma \rightarrow K_S K_S$. The values marked with stars are fixed by using other data.

	First nonet			Second nonet		
	$a_2(1320)$	$f_2(1270)$	$f'_2(1525)$	$a_2(1730)$	$f_2(1560)$	$f_2(1750)$
Mass (MeV)	1304 ± 10	1277 ± 6	1523 ± 5	1730^*	1570^*	1755 ± 10
Width (MeV)	120 ± 15	195 ± 15	104 ± 10	340^*	160^*	67 ± 12
g^L (GeV)	0.8 ± 0.1	0.9 ± 0.1	1.05 ± 0.1	0.38 ± 0.05		
φ (deg)	-1 ± 3			-10^{+5}_{-10}		

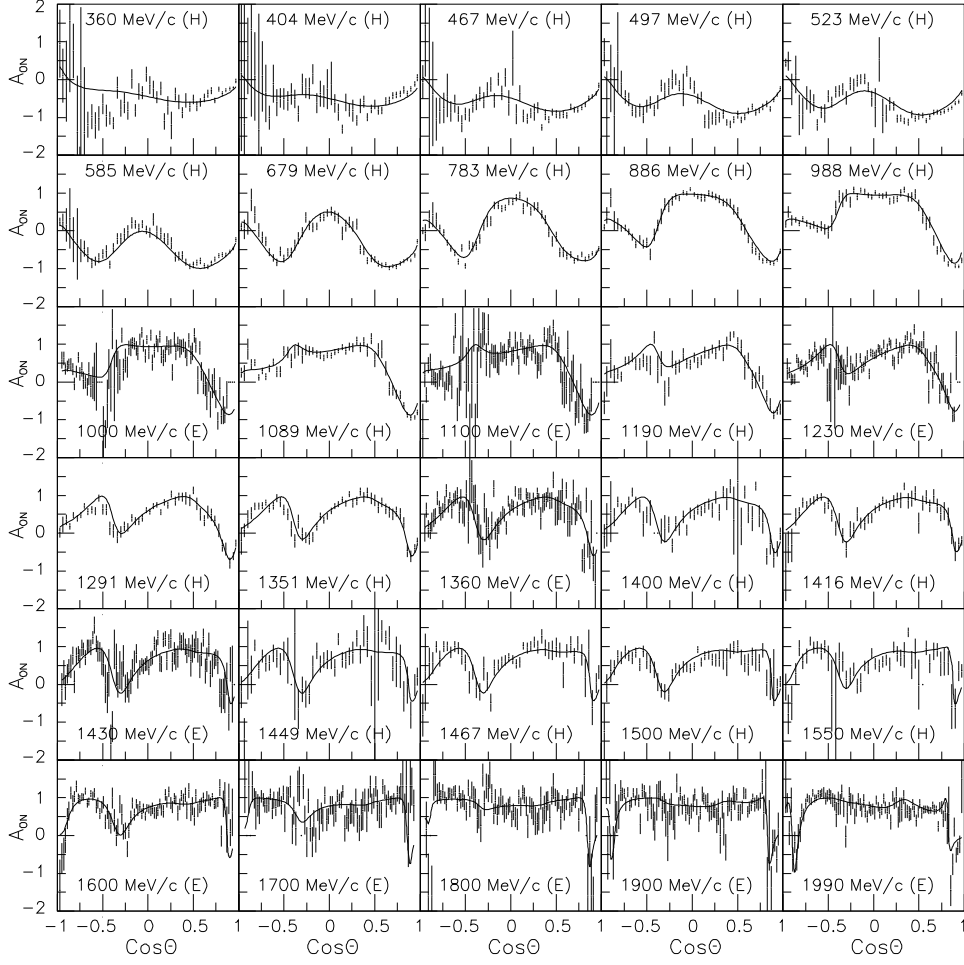


Figure 8: Polarisation in $p\bar{p} \rightarrow \pi^+\pi^-$ [42] and its fit within resonances of Eq. (2).

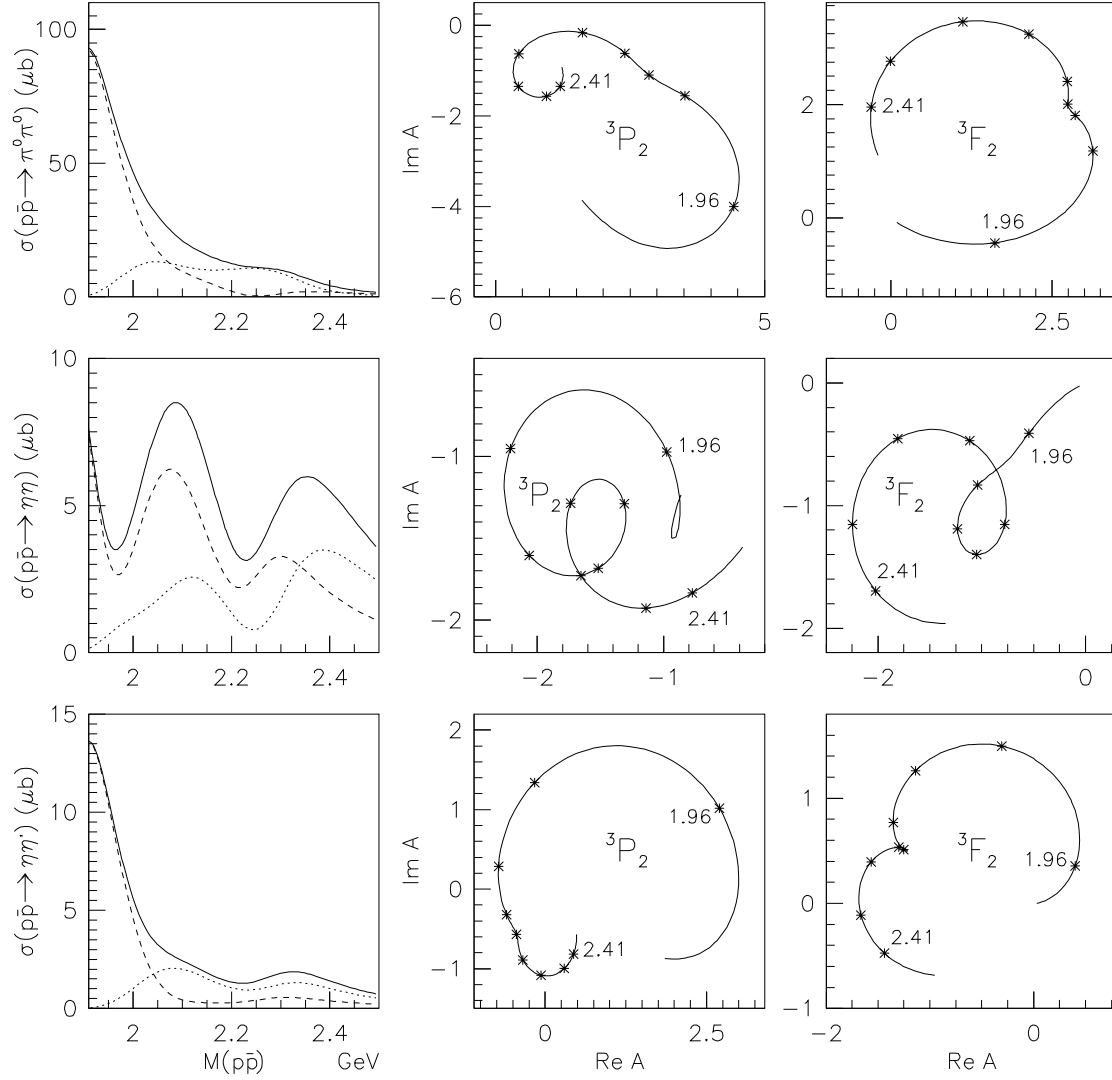


Figure 9: Cross sections and Argand-plots for 3P_2 and 3F_2 waves in the reaction $p\bar{p} \rightarrow \pi^0\pi^0, \eta\eta, \eta\eta'$. The upper row refers to $p\bar{p} \rightarrow \pi^0\pi^0$: we demonstrate the cross sections for 3P_2 and 3F_2 waves (dashed and dotted lines, respectively) and the total ($J = 2$) cross section (solid line) as well as Argand-plots for the 3P_2 and 3F_2 wave amplitudes at invariant masses $M = 1.962, 2.050, 2.100, 2.150, 2.200, 2.260, 2.304, 2.360, 2.410$ GeV. The figures in the second and third rows refer to the reactions $p\bar{p} \rightarrow \eta\eta$ and $p\bar{p} \rightarrow \eta\eta'$.

2.3 Data for proton-antiproton annihilation in flight $p\bar{p} \rightarrow \pi\pi, \eta\eta, \eta\eta'$

The $p\bar{p}$ annihilation in flight gives information about resonances with $M > 1900$ MeV. High statistical data taken at antiproton momenta 600, 900, 1150, 1200, 1350, 1525, 1640, 1800 and 1940 MeV/c were used for the analysis $p\bar{p} \rightarrow \pi^0\pi^0, \eta\eta, \eta\eta'$ [2]. The combined analysis was performed together with $\bar{p}p \rightarrow \pi^+\pi^-$ data obtained with a polarised target [42]. Five tensor states are required to describe the data, $f_2(1920), f_2(2000), f_2(2020), f_2(2240), f_2(2300)$:

Resonance	Mass(MeV)	Width(MeV)	(2)
$f_2(1920)$	1920 ± 30	230 ± 40	
$f_2(2000)$	2010 ± 30	495 ± 35	
$f_2(2020)$	2020 ± 30	275 ± 35	
$f_2(2240)$	2240 ± 40	245 ± 45	
$f_2(2300)$	2300 ± 35	290 ± 50	

The description of the data is illustrated by Figs. 5,6,7 and 8. In Fig. 9 we show the cross sections for $p\bar{p} \rightarrow \pi^0\pi^0, \eta\eta, \eta\eta'$ in $^3P_2\bar{p}p$ and $^3F_2\bar{p}p$ waves (dashed and dotted lines) and the total ($J = 2$) cross section (solid line) as well as Argand-plots for the 3P_2 and 3F_2 wave amplitudes at invariant masses $M = 1.962, 2.050, 2.100, 2.150, 2.200, 2.260, 2.304, 2.360, 2.410$ GeV.

The $\bar{p}p \rightarrow \pi^0\pi^0, \eta\eta, \eta\eta'$ amplitudes provide the following ratios for the f_2 resonance couplings $g_{\pi^0\pi^0} : g_{\eta\eta} : g_{\eta\eta'}$:

$f_2(1920)$	$1 : 0.56 \pm 0.08 : 0.41 \pm 0.07$	(3)
$f_2(2000)$	$1 : 0.82 \pm 0.09 : 0.37 \pm 0.22$	
$f_2(2020)$	$1 : 0.70 \pm 0.08 : 0.54 \pm 0.18$	
$f_2(2240)$	$1 : 0.66 \pm 0.09 : 0.40 \pm 0.14$	
$f_2(2300)$	$1 : 0.59 \pm 0.09 : 0.56 \pm 0.17$	

These coupling ratios allow one to estimate the quarkonium-gluonium c content of the f_2 - resonances.

3 Systematisation of tensor mesons on the (n, M^2) trajectories

In [11] (see also [5, 12]), the known $q\bar{q}$ -mesons consisting of light quarks ($q = u, d, s$) were put on the (n, M^2) trajectories, where n is the radial quantum number of the $q\bar{q}$ system with mass M . The trajectories for mesons with various quantum numbers turn out to be linear with a good accuracy:

$$M^2 = M_0^2 + (n - 1)\mu^2 \quad (4)$$

where $\mu^2 = 1.2 \pm 0.1 \text{ GeV}^2$ is a universal slope, and M_0 is the mass of the lowest state with $n = 1$.

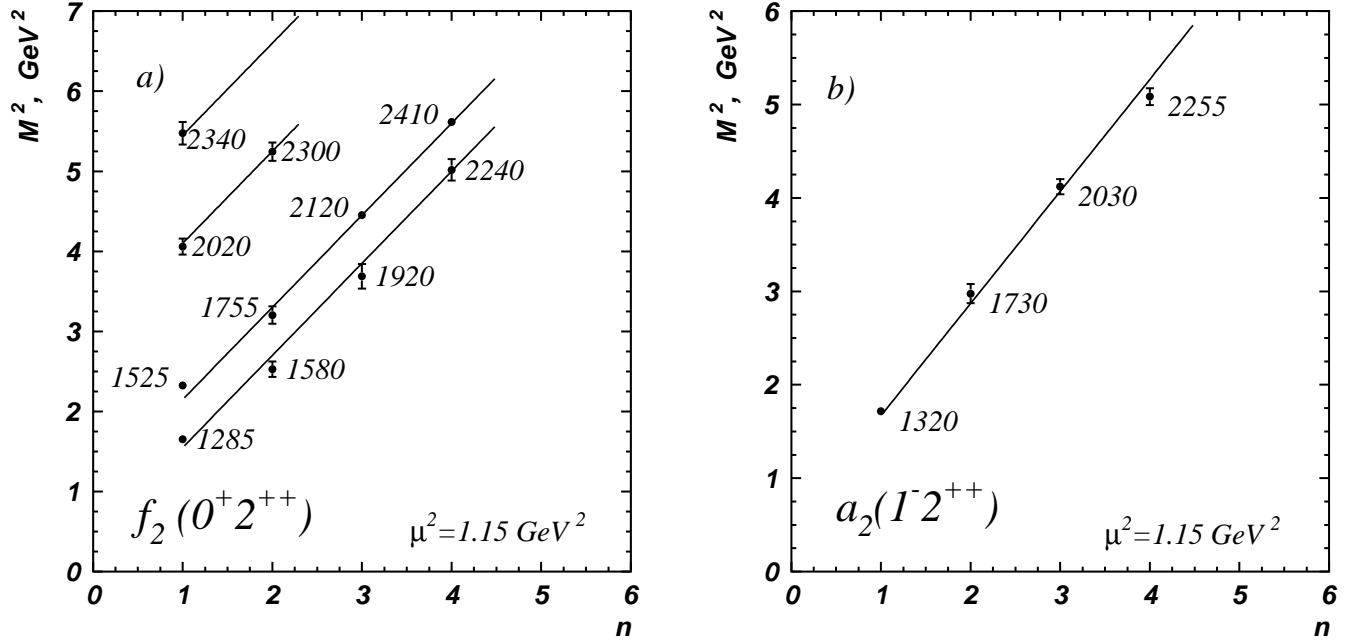


Figure 10: The f_2 and a_2 trajectories on the (n, M^2) plane; n is the radial quantum number of the $q\bar{q}$ state. The numbers stand for the experimentally observed f_2 and a_2 masses (M).

In Fig. 10a we demonstrate the present status of the (n, M^2) trajectories for the f_2 mesons (i.e. we use the results given by [2, 4, 6]). To avoid confusion, we list here the experimentally observable masses. First, it concerns the resonances seen in the $\phi\phi$ spectrum [7]. In [4] the $\phi\phi$ spectra were re-analysed, taking into account the existence of the broad $f_2(2000)$ resonance. As a result, the masses of three relatively narrow resonances are shifted compared to those given in the compilation PDG [1]:

$$f_2(2010)|_{PDG} \rightarrow f_2(2120) [4], \quad f_2(2300)|_{PDG} \rightarrow f_2(2340) [4], \quad f_2(2340)|_{PDG} \rightarrow f_2(2410) [4].$$

The trajectory for the a_2 -mesons, Fig. 10b, is drawn on the basis of the recent data [51].

The quark states with $(I = 0, J^{PC} = 2^{++})$ are determined by two flavour components $n\bar{n}$ and $s\bar{s}$ for which two states $^{2S+1}L_J = {}^3P_2, {}^3F_2$ are possible. Consequently, we have four trajectories on the (n, M^2) plane. Generally speaking, the f_2 -states are mixtures of both the flavour components and the $L = 1, 3$ waves. The real situation is, however, such that the lowest trajectory [$f_2(1275)$, $f_2(1580)$, $f_2(1920)$, $f_2(2240)$] consists of mesons with dominant ${}^3P_2 n\bar{n}$ components (we denote $n\bar{n} = (u\bar{u} + d\bar{d})/\sqrt{2}$), while the trajectory [$f_2(1525)$, $f_2(1755)$, $f_2(2120)$, $f_2(2410)$] contains mesons with predominantly ${}^3P_2 s\bar{s}$ components, and the F -trajectories are represented by three resonances [$f_2(2020)$, $f_2(2300)$] and [$f_2(2340)$] with the corresponding dominant ${}^3F_2 n\bar{n}$ and ${}^3F_2 s\bar{s}$ states. Following [9], we can state that the broad resonance $f_2(2000)$ is not part of those states placed on the (n, M^2) trajectories. In the region of 2000 MeV three $n\bar{n}$ -dominant resonances, $f_2(1920)$, $f_2(2000)$ and $f_2(2020)$, were seen, while on the (n, M^2) -trajectories there are only two vacant places. This means that one state is obviously "superfluous" from the

point of view of the $q\bar{q}$ -systematics, i.e. it has to be considered as exotics. The large value of the width of the $f_2(2000)$ strengthen the suspicion that, indeed, this state is an exotic one.

4 Quarkonium and gluonium states: mixing and decay

On the basis of the $1/N$ -expansion rules, we estimate here effects of mixing of quarkonium and gluonium states. Then, making use of the rules of quark combinatorics, we give the relations for decay constants of these states.

4.1 Mixing of $q\bar{q}$ and gg states

The rules of the $1/N$ -expansion [33, 34], where $N = N_c = N_f$ are numbers of colours and light flavours, provide a possibility to estimate the mixing of the gluonium (gg) with the neighbouring quarkonium states ($q\bar{q}$).

The admixture of the gg component in a $q\bar{q}$ -meson is small, of the order of $1/N_c$:

$$\begin{aligned} f_2(q\bar{q} - \text{meson}) &= q\bar{q} \cos \alpha + gg \sin \alpha \\ \sin^2 \alpha &\sim 1/N_c. \end{aligned} \quad (5)$$

The quarkonium component in the glueball should be larger, it is of the order of N_f/N_c :

$$\begin{aligned} f_2(\text{glueball}) &= gg \cos \gamma + (q\bar{q})_{\text{glueball}} \sin \gamma, \\ \sin^2 \gamma &\sim N_f/N_c, \end{aligned} \quad (6)$$

where $(q\bar{q})_{\text{glueball}}$ is a mixture of $n\bar{n} = (u\bar{u} + d\bar{d})/\sqrt{2}$ and $s\bar{s}$ components:

$$(q\bar{q})_{\text{glueball}} = n\bar{n} \cos \varphi_{\text{glueball}} + s\bar{s} \sin \varphi_{\text{glueball}}, \quad (7)$$

with $\sin \varphi_{\text{glueball}} = \sqrt{\lambda/(2 + \lambda)}$. If the flavour SU(3) symmetry were satisfied, the quarkonium component $(q\bar{q})_{\text{glueball}}$ would be a flavour singlet, $\varphi_{\text{glueball}} \rightarrow \varphi_{\text{singlet}} \simeq 37^\circ$. In reality, the probability of strange quark production in a gluon field is suppressed: $u\bar{u} : d\bar{d} : s\bar{s} = 1 : 1 : \lambda$, where $\lambda \simeq 0.5 - 0.85$. Hence, $(q\bar{q})_{\text{glueball}}$ differs slightly from the flavour singlet, it is determined by the parameter λ as follows [43]:

$$(q\bar{q})_{\text{glueball}} = (u\bar{u} + d\bar{d} + \sqrt{\lambda} s\bar{s})/\sqrt{2 + \lambda}. \quad (8)$$

The suppression parameter λ was estimated both in multiple hadron production processes [44], and in hadronic decay processes [45, 26]. In hadronic decays of mesons with different J^{PC} the value of λ can be, in principle, different. Still, the analyses of the decays of the 2^{++} -states [45] and 0^{++} -states [26] show that the suppression parameters are of the same order, 0.5–0.85, leading to

$$\varphi_{\text{glueball}} \simeq 26^\circ - 33^\circ. \quad (9)$$

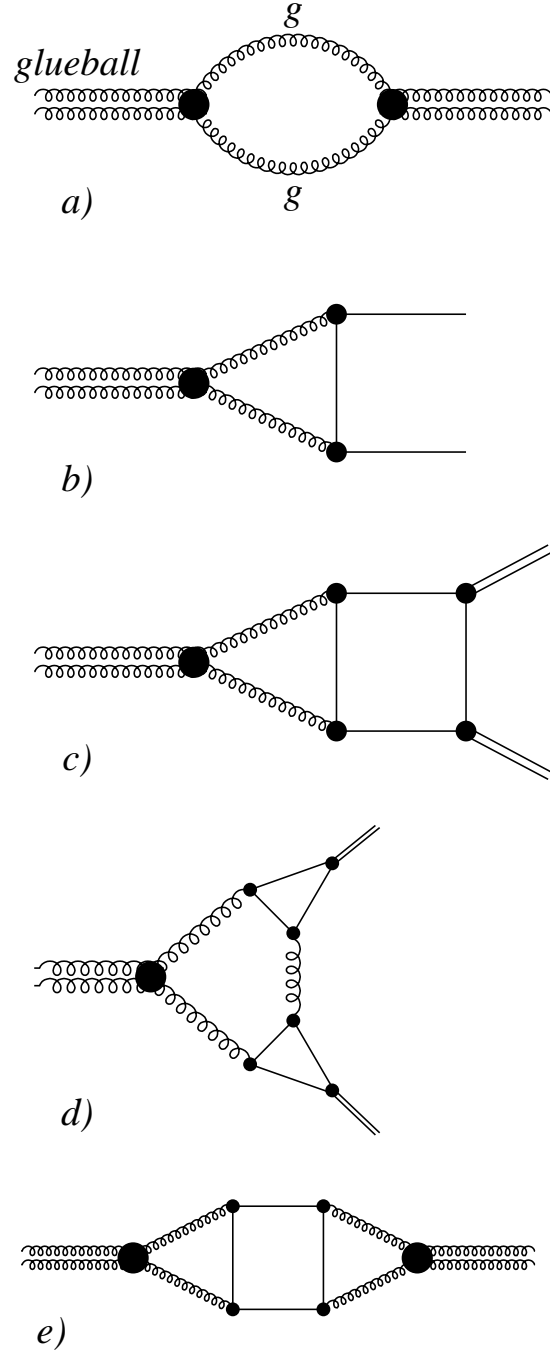


Figure 11: Examples of the diagrams which determine gluonium (gg) decay.

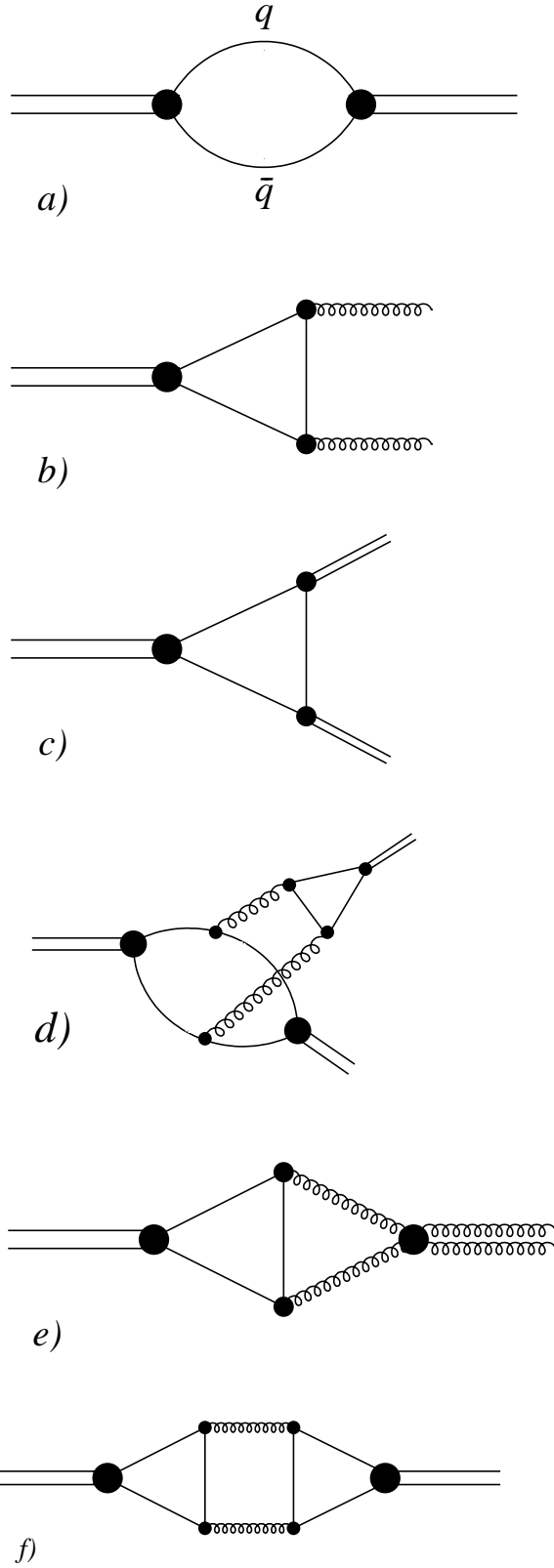


Figure 12: Examples of the diagrams which determine quarkonium ($q\bar{q}$) decay.

Let us explain now Eqs. (5)-(8) in detail.

First, let us evaluate the transition couplings using the rules of $1/N$ -expansion; this evaluation will be done for the decay transitions *gluonium* \rightarrow *two $q\bar{q}$ -mesons* and *quarkonium* \rightarrow *two $q\bar{q}$ -mesons*. For this purpose, we consider the gluon loop diagram which corresponds to the two-gluon self-energy part: *gluonium* \rightarrow *two gluons* \rightarrow *gluonium* (see Fig. 11a). This loop diagram $B(\text{gluonium} \rightarrow gg \rightarrow \text{gluonium})$ is of the order of unity, provided the gluonium is a two-gluon composite system: $B(\text{gluonium} \rightarrow gg \rightarrow \text{gluonium}) \sim g_{\text{gluonium} \rightarrow gg}^2 N_c^2 \sim 1$, where $g_{\text{gluonium} \rightarrow gg}$ is a coupling constant for the transition of a gluonium to two gluons. Therefore,

$$g_{\text{gluonium} \rightarrow gg} \sim 1/N_c. \quad (10)$$

The coupling constant for the *gluonium* \rightarrow *$q\bar{q}$* transition is determined by the diagrams of Fig. 11b type. A similar evaluation gives:

$$g_{\text{gluonium} \rightarrow q\bar{q}} \sim g_{\text{gluonium} \rightarrow gg} g^2 N_c \sim 1/N_c. \quad (11)$$

Here g is the quark-gluon coupling constant, which is of the order of $1/\sqrt{N_c}$ [33]. The coupling constant for the *gluonium* \rightarrow *two $q\bar{q}$ -mesons* transition in the leading $1/N_c$ terms is governed by diagrams of Fig. 11c type:

$$g_{\text{gluonium} \rightarrow \text{two mesons}}^L \sim g_{\text{gluonium} \rightarrow q\bar{q}} g_{\text{meson} \rightarrow q\bar{q}}^2 N_c \sim 1/N_c. \quad (12)$$

In (12) the following evaluation of the coupling for transition *$q\bar{q}$ -meson* \rightarrow *$q\bar{q}$* has been used:

$$g_{\text{meson} \rightarrow q\bar{q}} \sim 1/\sqrt{N_c}, \quad (13)$$

which follows from the fact that the loop diagram of the *$q\bar{q}$ -meson* propagator (see Fig. 12a) is of the order of unity: $B(q\bar{q} - \text{meson} \rightarrow q\bar{q} \rightarrow \text{meson}) \sim g_{\text{meson} \rightarrow q\bar{q}}^2 N_c \sim 1$.

The diagram of the type of Fig. 11d governs the couplings for the transition *gluonium* \rightarrow *two $q\bar{q}$ -mesons* in the next-to-leading terms of the $1/N_c$ -expansion:

$$g_{\text{gluonium} \rightarrow \text{two mesons}}^{NL} \sim g_{\text{gluonium} \rightarrow gg} g_{\text{meson} \rightarrow gg}^2 N_c^2 \sim 1/N_c^2, \quad (14)$$

where the coupling $g_{\text{meson} \rightarrow gg}$ has been estimated following the diagram in Fig. 12b:

$$g_{\text{meson} \rightarrow gg} \sim g_{\text{meson} \rightarrow q\bar{q}} g^2 \sim 1/N_c^{3/2}. \quad (15)$$

Decay couplings of *$q\bar{q}$ -meson* into two mesons in leading and next-to-leading terms of $1/N_c$ expansion are determined by diagrams of the type of Figs. 12c and 12d, respectively. This gives

$$\begin{aligned} g_{\text{meson} \rightarrow \text{two mesons}}^L &\sim g_{\text{meson} \rightarrow q\bar{q}}^3 N_c \sim 1/\sqrt{N_c}, \\ g_{\text{meson} \rightarrow \text{two mesons}}^{NL} &\sim g_{\text{meson} \rightarrow q\bar{q}}^2 g_{\text{meson} \rightarrow gg} g^2 N_c^2 \sim 1/N_c^{3/2}. \end{aligned} \quad (16)$$

Now we can estimate the order of the value of $\sin^2 \gamma$ which defines the probability $(q\bar{q})_{\text{glueball}}$, see Eq. (6). This probability is determined by the self-energy part of the gluon propagator

(diagram in Fig. 11e)—it is of the order of N_f/N_c , the factor N_f being the light flavour number in the quark loop. Let us emphasise that the diagram in Fig. 11e stands for only one of the contributions of that type; indeed, contributions of the same order are also given by diagrams with all possible (but planar) gluon exchanges in the quark loop.

One can also evaluate $\sin^2 \gamma$ using the transition amplitude *gluonium* \rightarrow *quarkonium* (see Fig. 12e), which is of the order of $1/\sqrt{N_c}$. The value $\sin^2 \gamma$ is determined by the transition amplitude squared, summed over the flavours of all quarkonia, thus resulting in Eq. (6).

The probability of the gluonium component in the quarkonium, $\sin^2 \alpha$, is of the order of the diagram in Fig. 12f, $\sim 1/N_c$, giving us the estimate (5). Here, as in the self-energy gluonium block, planar-type gluon exchanges are possible. Because of this, in the intermediate $q\bar{q}$ state all the interactions are taken into account.

The diagram in Fig. 11e defines also the flavour content of $(q\bar{q})_{\text{glueball}}$ — we see that the gluon field produces light quark pairs with probabilities $u\bar{u} : d\bar{d} : s\bar{s} = 1 : 1 : \lambda$, so $(q\bar{q})_{\text{glueball}}$ is determined by Eq. (8) not being a flavour singlet.

4.2 Quark combinatorial relations for decay constants

The rules of quark combinatorics lead to relations between decay couplings for mesons which belong to the same SU(3) nonet. The violation of the flavour symmetry is taken into account by introducing a suppression parameter λ for the production of the strange quarks by gluons.

In the leading terms of the $1/N$ expansion, the main contribution to the decay coupling constant comes from planar diagrams. Examples of the production of new $q\bar{q}$ -pairs by intermediate gluons are shown in Figs. 13a and 12b. When an isoscalar $q\bar{q}$ -meson disintegrates, the coupling constants can be determined up to a common factor, by two characteristics of a meson. The first is the quark content of the $q\bar{q}$ -meson, $q\bar{q} = n\bar{n} \cos \varphi + s\bar{s} \sin \varphi$, the second is the parameter λ . Experimental data provide the following values for this parameter: $\lambda \simeq 0.5$ [44] in central hadron production in high-energy hadron-hadron collisions, $\lambda = 0.8 \pm 0.2$ [45] for the decays of tensor mesons and $\lambda = 0.5 - 0.9$ [26] for the decays of 0^{++} mesons.

Let us consider in more detail the production of two pseudoscalar mesons $P_1 P_2$ by f_2 -quarkonium and f_2 -gluonium:

$$\begin{aligned} f_2(\text{quarkonium}) &\rightarrow \pi\pi, K\bar{K}, \eta\eta, \eta\eta', \eta'\eta' \\ f_2(\text{gluonium}) &\rightarrow \pi\pi, K\bar{K}, \eta\eta, \eta\eta', \eta'\eta'. \end{aligned} \quad (17)$$

The coupling constants for the decay into channels (17), which in the leading terms of the $1/N$ expansion are determined by diagrams of the type shown in Fig. 13, may be presented as

$$\begin{aligned} g^L(q\bar{q} \rightarrow P_1 P_2) &= C_{P_1 P_2}^{q\bar{q}}(\varphi, \lambda) g_P^L, \\ g^L(gg \rightarrow P_1 P_2) &= C_{P_1 P_2}^{gg}(\lambda) G_P^L, \end{aligned} \quad (18)$$

where $C_{P_1 P_2}^{q\bar{q}}(\varphi, \lambda)$ and $C_{P_1 P_2}^{gg}(\lambda)$ are wholly calculable coefficients depending on the mixing angle φ and parameter λ ; g_P^L and G_P^L are common factors describing the unknown dynamics of the processes.

Dealing with processes of the Fig. 13b type, one should bear in mind that they do not contain $(q\bar{q})_{\text{quarkonium}}$ components in the intermediate state but $(q\bar{q})_{\text{continuous spectrum}}$ only. The states $(q\bar{q})_{\text{quarkonium}}$ in this diagram would lead to processes of Fig. 13c, namely, to a diagram with the quarkonium decay vertex and the mixing block of gg and $q\bar{q}$ components. All these sub-processes are taken into account separately.

The contributions of the diagrams of the type of Fig. 11d and 12d, which give the next-to-leading terms, $g^{NL}(q\bar{q} \rightarrow P_1 P_2)$ and $g^{NL}(gg \rightarrow P_1 P_2)$, may be presented in a form analogous to (18). The decay constant to the channel $P_1 P_2$ is a sum of both contributions:

$$\begin{aligned} g^L(q\bar{q} \rightarrow P_1 P_2) &+ g^{NL}(q\bar{q} \rightarrow P_1 P_2), \\ g^L(gg \rightarrow P_1 P_2) &+ g^{NL}(gg \rightarrow P_1 P_2). \end{aligned} \tag{19}$$

The second terms are suppressed compared to the first ones by a factor N_c ; the experience in the calculation of quark diagrams teaches us that this suppression is of the order of 1/10.

Coupling constants for gluonium decays, $g^L(gg \rightarrow P_1 P_2)$ and $g^{NL}(gg \rightarrow P_1 P_2)$, are presented in Table 3 while those for quarkonium decays, $g^L(q\bar{q} \rightarrow P_1 P_2)$ and $g^{NL}(q\bar{q} \rightarrow P_1 P_2)$, are given in Table 4.

In Table 5 we give the couplings for decays of the gluonium state into channels of the vector mesons: $gg \rightarrow V_1 V_2$.

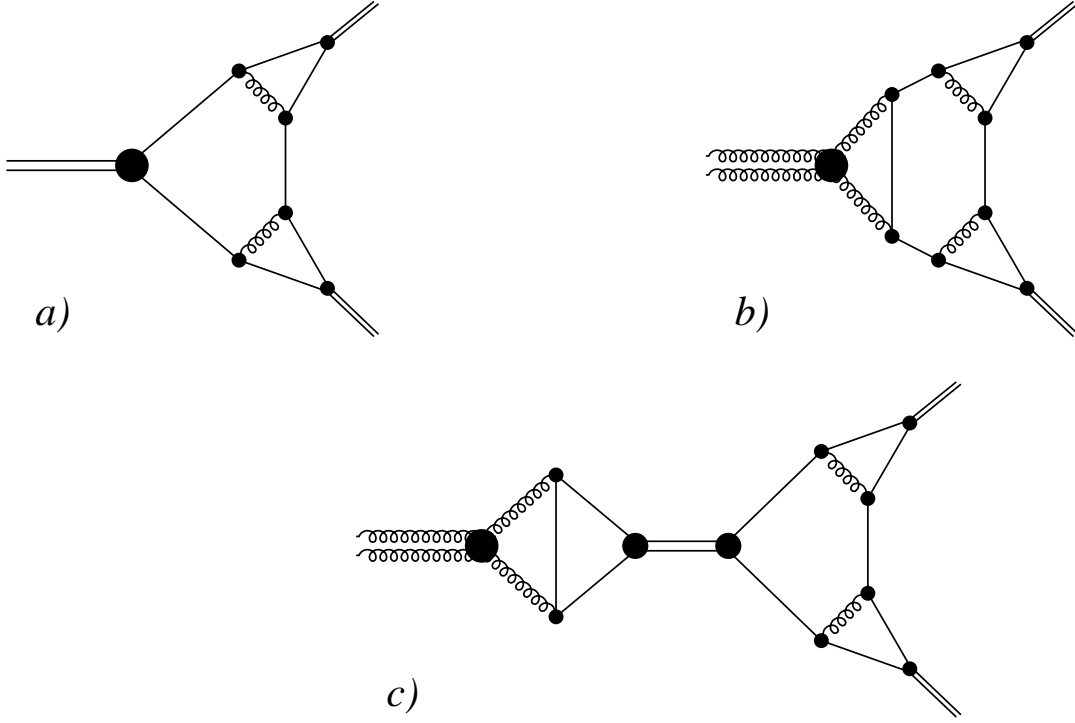


Figure 13: Examples of planar diagrams responsible for the decay of the $q\bar{q}$ -state (a) and the gluonium (b) into two $q\bar{q}$ -mesons (leading terms in the $1/N$ expansion). c) Diagram for the gluonium decay with a pole in the intermediate $q\bar{q}$ -state: this process is not included into the gluonium decay vertex.

Table 3

Coupling constants of the f_2 -gluonium decaying to two pseudoscalar mesons, in the leading and next-to leading terms of $1/N$ expansion. Θ is here the mixing angle for $\eta - \eta'$ mesons:
 $\eta = n\bar{n} \cos \Theta - s\bar{s} \sin \Theta$ and $\eta' = n\bar{n} \sin \Theta + s\bar{s} \cos \Theta$.

Channel	Gluonium decay couplings in the leading term of $1/N$ expansion.	Gluonium decay couplings in the next-to-leading term of $1/N$ expansion.	Identity factor
$\pi^0\pi^0$	G^L	0	1/2
$\pi^+\pi^-$	G^L	0	1
K^+K^-	$\sqrt{\lambda}G^L$	0	1
$K^0\bar{K}^0$	$\sqrt{\lambda}G^L$	0	1
$\eta\eta$	$G^L (\cos^2 \Theta + \lambda \sin^2 \Theta)$	$2G^{NL}(\cos \Theta - \sqrt{\frac{\lambda}{2}} \sin \Theta)^2$	1/2
$\eta\eta'$	$G^L(1 - \lambda) \sin \Theta \cos \Theta$	$2G^{NL}(\cos \Theta - \sqrt{\frac{\lambda}{2}} \sin \Theta) \times (\sin \Theta + \sqrt{\frac{\lambda}{2}} \cos \Theta)$	1
$\eta'\eta'$	$G^L (\sin^2 \Theta + \lambda \cos^2 \Theta)$	$2G^{NL} (\sin \Theta + \sqrt{\frac{\lambda}{2}} \cos \Theta)^2$	1/2

Table 4

Coupling constants of the f_2 -quarkonium decaying to two pseudoscalar mesons in the leading and next-to-leading terms of the $1/N$ expansion. The flavour content of the f_2 -quarkonium is determined by the mixing angle φ as follows: $f_2(q\bar{q}) = n\bar{n} \cos \varphi + s\bar{s} \sin \varphi$ where $n\bar{n} = (u\bar{u} + d\bar{d})/\sqrt{2}$.

Channel	Decay couplings of quarkonium in leading term of $1/N$ expansion.	Decay couplings of quarkonium in next-to-leading term of $1/N$ expansion.
$\pi^0\pi^0$	$g^L \cos \varphi/\sqrt{2}$	0
$\pi^+\pi^-$	$g^L \cos \varphi/\sqrt{2}$	0
K^+K^-	$g^L(\sqrt{2} \sin \varphi + \sqrt{\lambda} \cos \varphi)/\sqrt{8}$	0
$K^0\bar{K}^0$	$g^L(\sqrt{2} \sin \varphi + \sqrt{\lambda} \cos \varphi)/\sqrt{8}$	0
$\eta\eta$	$g^L \left(\cos^2 \Theta \cos \varphi/\sqrt{2} + \sqrt{\lambda} \sin \varphi \sin^2 \Theta \right)$	$\sqrt{2}g^{NL}(\cos \Theta - \sqrt{\frac{\lambda}{2}} \sin \Theta) \times (\cos \varphi \cos \Theta - \sin \varphi \sin \Theta)$
$\eta\eta'$	$g^L \sin \Theta \cos \Theta \left(\cos \varphi/\sqrt{2} - \sqrt{\lambda} \sin \varphi \right)$	$\sqrt{\frac{1}{2}}g^{NL} \left[(\cos \Theta - \sqrt{\frac{\lambda}{2}} \sin \Theta) \times (\cos \varphi \sin \Theta + \sin \varphi \cos \Theta) + (\sin \Theta + \sqrt{\frac{\lambda}{2}} \cos \Theta) \times (\cos \varphi \sin \Theta - \sin \varphi \cos \Theta) \right]$
$\eta'\eta'$	$g^L \left(\sin^2 \Theta \cos \varphi/\sqrt{2} + \sqrt{\lambda} \sin \varphi \cos^2 \Theta \right)$	$\sqrt{2}g^{NL}(\sin \Theta + \sqrt{\frac{\lambda}{2}} \cos \Theta) \times (\cos \varphi \cos \Theta + \sin \varphi \sin \Theta)$

Table 5

The constants of the tensor glueball decay into two vector mesons in the leading (planar diagrams) and next-to-leading (non-planar diagrams) terms of $1/N$ -expansion. The mixing angle for $\omega - \phi$ mesons is defined as: $\omega = n\bar{n} \cos \varphi_V - s\bar{s} \sin \varphi_V$, $\phi = n\bar{n} \sin \varphi_V + s\bar{s} \cos \varphi_V$.

Because of the small value of φ_V , we keep in the Table only terms of the order of φ_V .

Channel	Constants for glueball decays in the leading order of $1/N$ expansion	Constants for glueball decays in next-to-leading order of $1/N$ expansion	Identity factor for decay products
$\rho^0 \rho^0$	G_V^L	0	1/2
$\rho^+ \rho^-$	G_V^L	0	1
$K^{*+} K^{*-}$	$\sqrt{\lambda} G_V^L$	0	1
$K^{*0} \bar{K}^{*0}$	$\sqrt{\lambda} G_V^L$	0	1
$\omega \omega$	G_V^L	$2G_V^{NL}$	1/2
$\omega \phi$	$G_V^L (1 - \lambda) \varphi_V$	$2G_V^{NL} \left(\sqrt{\frac{\lambda}{2}} + \varphi_V \left(1 - \frac{\lambda}{2} \right) \right)$	1
$\phi \phi$	λG_V^L	$2G_V^{NL} \left(\frac{\lambda}{2} + \sqrt{2\lambda} \varphi_V \right)$	1/2

5 The broad state $f_2(2000)$: the tensor glueball

In the leading terms of $1/N_c$ -expansion we have definite ratios for the glueball decay couplings. The next-to-leading terms in the decay couplings give corrections of the order of $1/N_c$. Let us remind that, as we see in the numerical calculations of the diagrams, the $1/N_c$ factor leads to a smallness of the order of $1/10$, and we neglect them in the analysis of the decays $f_2 \rightarrow \pi^0 \pi^0, \eta \eta, \eta \eta'$.

Considering a glueball state which is also a mixture of the gluonium and quarkonium components, we have $\varphi \rightarrow \varphi_{glueball} = \sin^{-1} \sqrt{\lambda/(2 + \lambda)}$ for the latter. So we can write

$$\frac{g^L((q\bar{q})_{glueball} \rightarrow P_1 P_2)}{g^L((q\bar{q})_{glueball} \rightarrow P'_1 P'_2)} = \frac{g^L(gg \rightarrow P_1 P_2)}{g^L(gg \rightarrow P'_1 P'_2)} \quad (20)$$

Then the relations for decay couplings of the glueball in the leading terms of the $1/N$ -expansion read:

$$\begin{aligned} g_{\pi^0 \pi^0}^{glueball} &= \frac{G_{glueball}^L}{\sqrt{2 + \lambda}}, \\ g_{\eta \eta}^{glueball} &= \frac{G_{glueball}^L}{\sqrt{2 + \lambda}} (\cos^2 \Theta + \lambda \sin^2 \Theta) \\ g_{\eta \eta'}^{glueball} &= \frac{G_{glueball}^L}{\sqrt{2 + \lambda}} (1 - \lambda) \sin \Theta \cos \Theta. \end{aligned} \quad (21)$$

Hence, in spite of the unknown quarkonium components in the glueball, there are definite

relations between the couplings of the glueball state with the channels $\pi^0\pi^0, \eta\eta, \eta\eta'$ which can serve as signatures to define it.

5.1 Ratios between coupling constants of $f_2(2000) \rightarrow \pi^0\pi^0, \eta\eta, \eta\eta'$ as indication of a glueball nature of this state

Eq. (21) tells us that for the glueball state the relations between the coupling constants are $1 : (\cos^2 \Theta + \lambda \sin^2 \Theta) : (1 - \lambda) \cos \Theta \sin \Theta$. For $(\lambda = 0.5, \Theta = 37^\circ)$ we have $1 : 0.82 : 0.24$, and for $(\lambda = 0.85, \Theta = 37^\circ)$, respectively, $1 : 0.95 : 0.07$. Consequently, the relations between the coupling constants $g_{\pi^0\pi^0} : g_{\eta\eta} : g_{\eta\eta'}$ for the glueball have to be

$$2^{++} \text{ glueball} \quad g_{\pi^0\pi^0} : g_{\eta\eta} : g_{\eta\eta'} = 1 : (0.82 - 0.95) : (0.24 - 0.07). \quad (22)$$

It follows from (3) that only the coupling constants of the broad $f_2(2000)$ resonance are inside the intervals: $0.82 \leq g_{\eta\eta}/g_{\pi^0\pi^0} \leq 0.95$ and $0.24 \geq g_{\eta\eta'}/g_{\pi^0\pi^0} \geq 0.07$. Hence, it is just this resonance which can be considered as a candidate for a tensor glueball, while λ is fixed in the interval $0.5 \leq \lambda \leq 0.7$. Taking into account that there is no place for $f_2(2000)$ on the (n, M^2) -trajectories (see Fig. 10), it becomes evident that indeed, this resonance is the lowest tensor glueball.

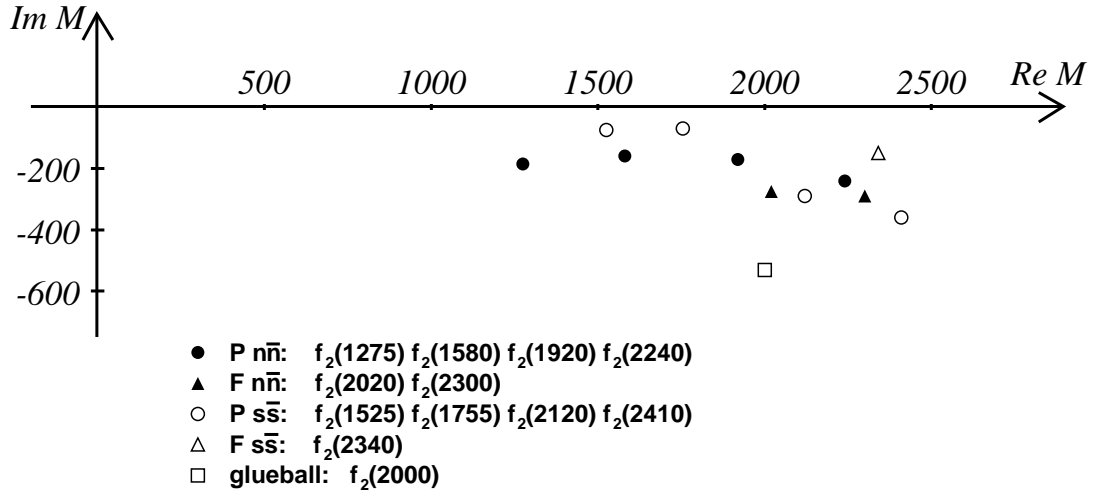


Figure 14: Position of the f_2 -poles in the complex- M plane: states with dominant ${}^3P_2 n\bar{n}$ -component (full circle), ${}^3F_2 n\bar{n}$ -component (full triangle), ${}^3P_2 s\bar{s}$ -component (open circle), ${}^3F_2 s\bar{s}$ -component (open triangle), glueball (open square).

5.2 Mixing of the glueball with neighbouring $q\bar{q}$ -resonances

The position of the f_2 -poles on the complex M -plane is shown in Fig. 14. We see that the glueball state $f_2(2000)$ overlaps with a large group of $q\bar{q}$ -resonances. This means that there is

a considerable mixing with the neighbouring resonances. The mixing can take place both at relatively small distances, on the quark-gluon level (processes of the type shown in Fig. 12e), and owing to decay processes

$$f_2(\text{glueball}) \rightarrow \text{real mesons} \rightarrow f_2(q\bar{q} - \text{meson}). \quad (23)$$

Processes of the type of (23) are presented in Fig. 15.

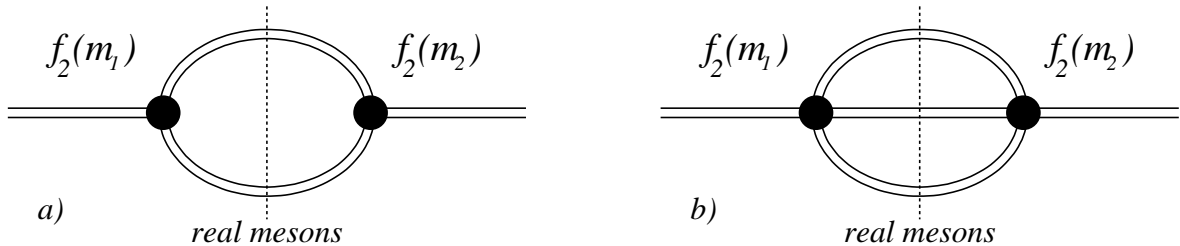


Figure 15: Transitions $f_2(m_1) \rightarrow \text{real mesons} \rightarrow f_2(m_2)$, responsible for the accumulation of widths in the case of overlapping resonances.

The estimates which were carried out in Section 4 demonstrated that even the mixing at the quark-gluon level (diagrams of the types in Fig. 12e) leads to a sufficiently large admixture of the quark-antiquark component in the glueball: $f_2(\text{glueball}) = \cos \gamma gg + \sin \gamma q\bar{q}$ with $\sin \gamma \sim \sqrt{N_f/N_c}$. A mixing due to processes (23), apparently, enhances the quark-antiquark component. The main effect of the processes (23) is, however, that in the case of overlapping resonances one of them accumulates the widths of the neighbouring resonances. The position of the f_2 -poles in Fig. 14 makes it obvious that such a state is the tensor glueball.

A similar situation was detected also in the sector of scalar mesons in the region 1000 – 1700 MeV: the scalar glueball, being in the neighbourhood of $q\bar{q}$ -resonances, accumulated a relevant fraction of their widths and transformed into a broad $f_0(1200 - 1600)$ state. Such a transformation of a scalar glueball into a broad state was observed in [12, 26]; further investigations verified this observation. The possibility that a scalar (and tensor) glueball may considerably mix with $q\bar{q}$ -states was discussed already for quite a long time, see, e.g., [32, 35, 36]. At the same time there is a number of papers, e.g. [35, 36], in which the mixing due to transitions (23) is not taken into account. Hence, in these papers relatively narrow resonances like $f_0(1500)$ and $f_0(1710)$ are suggested as possible scalar glueballs.

We see that both glueballs, the scalar $f_0(1200 - 1600)$ and the tensor $f_2(2000)$ one, reveal themselves as broad resonances. We can suppose that this is not accidental. In [15] the transition of the lowest scalar glueball into a broad resonance was investigated in the framework of modelling decays by self-energy quark and gluon diagrams. As it was discovered, it was just the glueball which, appearing among the $q\bar{q}$ -states, began to mix with them actively, accumulating their widths. Hence, the glueball turned out to be the broadest resonance.

5.2.1 The mixing of two unstable states

In the case of two resonances, the propagator of the state 1 is determined by the diagrams of Fig. 16a. With all these processes taken into account, the propagator of the state 1 is equal to:

$$D_{11}(s) = \left(m_1^2 - s - B_{11}(s) - \frac{B_{12}(s)B_{21}(s)}{m_2^2 - s - B_{22}(s)} \right)^{-1}. \quad (24)$$

Here m_1 and m_2 are masses of the input states 1 and 2, and the loop diagrams $B_{ij}(s)$ are defined by the spectral integral

$$B_{ij}(s) = \int_{4m^2}^{\infty} \frac{d(s')}{\pi} \frac{g_i(s')g_j(s')\rho(s')}{s' - s - i0}, \quad (25)$$

where $g_i(s')$ and $g_j(s')$ are vertices and $\rho(s')$ is the phase space for the intermediate state. It is helpful to introduce the propagator matrix D_{ij} , where the non-diagonal elements $D_{12} = D_{21}$ correspond to the transitions $1 \rightarrow 2$ and $2 \rightarrow 1$ (see Fig. 16b). The matrix reads:

$$\hat{D} = \begin{vmatrix} D_{11} & D_{12} \\ D_{21} & D_{22} \end{vmatrix} = \frac{1}{(M_1^2 - s)(M_2^2 - s) - B_{12}B_{21}} \begin{vmatrix} M_2^2 - s, & B_{12} \\ B_{21}, & M_1^2 - s \end{vmatrix}. \quad (26)$$

Here the following notation is used:

$$M_i^2 = m_i^2 - B_{ii}(s) \quad i = 1, 2. \quad (27)$$

Zeros in the denominator of the propagator matrix (26) define the complex resonance masses after the mixing:

$$\Pi(s) = (M_1^2 - s)(M_2^2 - s) - B_{12}B_{21} = 0. \quad (28)$$

Let us denote the complex masses of mixed states as M_A and M_B .

Consider a simple model, where the s -dependence of the function $B_{ij}(s)$ near the points $s \sim M_A^2$ and $s \sim M_B^2$ is assumed to be negligible. Let M_i^2 and B_{12} be constants. Then one has:

$$M_{A,B}^2 = \frac{1}{2}(M_1^2 + M_2^2) \pm \sqrt{\frac{1}{4}(M_1^2 - M_2^2)^2 + B_{12}B_{21}}. \quad (29)$$

In the case, when the widths of initial resonances 1 and 2 are small (hence the imaginary part of the transition diagram B_{12} is also small), the equation (29) turns into the standard formula of quantum mechanics for the split of mixing levels, which become repulsive as a result of the mixing. If so,

$$\hat{D} = \begin{vmatrix} \cos^2 \theta / (M_A^2 - s) + \sin^2 \theta / (M_B^2 - s) & -\cos \theta \sin \theta / (M_A^2 - s) + \sin \theta \cos \theta / (M_B^2 - s) \\ -\cos \theta \sin \theta / (M_A^2 - s) + \sin \theta \cos \theta / (M_B^2 - s) & \sin^2 \theta / (M_A^2 - s) + \cos^2 \theta / (M_B^2 - s) \end{vmatrix},$$

$$\cos^2 \theta = \frac{1}{2} + \frac{1}{2} \frac{\frac{1}{2}(M_1^2 - M_2^2)}{\sqrt{\frac{1}{4}(M_1^2 - M_2^2)^2 + B_{12}B_{21}}}. \quad (30)$$

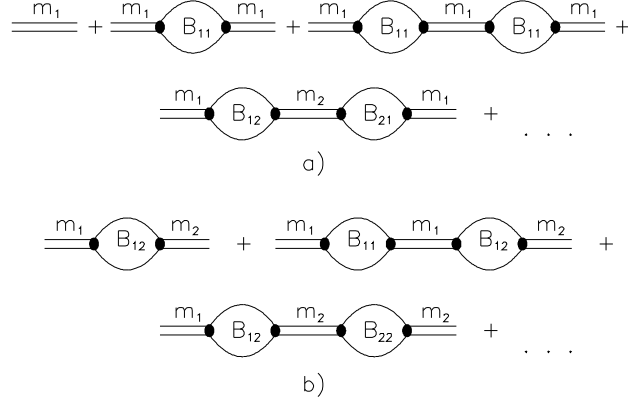


Figure 16: Diagrams describing the propagation functions D_{11} (a) and D_{12} (b) for the interaction of two resonance states.

The states $|A\rangle$ and $|B\rangle$ are superpositions of the initial levels, $|1\rangle$ and $|2\rangle$, as follows:

$$|A\rangle = \cos\theta|1\rangle - \sin\theta|2\rangle, \quad |B\rangle = \sin\theta|1\rangle + \cos\theta|2\rangle. \quad (31)$$

In general, the representation of states $|A\rangle$ and $|B\rangle$ as superpositions of initial states is valid, when the s -dependence of functions $B_{ij}(s)$ can not be neglected, and their imaginary parts are not small. Consider the propagator matrix near $s = M_A^2$:

$$\hat{D} = \frac{1}{\Pi(s)} \begin{vmatrix} M_2^2(s) - s & B_{12}(s) \\ B_{21}(s) & M_1^2(s) - s \end{vmatrix} \simeq \frac{-1}{\Pi'(M_A^2)(M_A^2 - s)} \begin{vmatrix} M_2^2(M_A^2) - M_A^2 & B_{12}(M_A^2) \\ B_{21}(M_A^2) & M_1^2(M_A^2) - M_A^2 \end{vmatrix}. \quad (32)$$

In the left-hand side of Eq. (32), only the singular (pole) terms survive. The matrix determinant in the right-hand side of (32) equals zero:

$$[M_2^2(M_A^2) - M_A^2][M_1^2(M_A^2) - M_A^2] - B_{12}(M_A^2)B_{21}(M_A^2) = 0, \quad (33)$$

This equality follows from Eq. (28), which fixes $\Pi(M_A^2) = 0$. It allows us to introduce the complex mixing angle:

$$|A\rangle = \cos\theta_A|1\rangle - \sin\theta_A|2\rangle. \quad (34)$$

The right-hand side of Eq. (30) can be rewritten by making use of the mixing angle θ_A , as follows:

$$[\hat{D}]_{s \sim M_A^2} = \frac{N_A}{M_A^2 - s} \begin{vmatrix} \cos^2\theta_A & -\cos\theta_A \sin\theta_A \\ -\sin\theta_A \cos\theta_A & \sin^2\theta_A \end{vmatrix}, \quad (35)$$

where

$$N_A = \frac{1}{\Pi'(M_A^2)} [2M_A^2 - M_1^2 - M_2^2], \cos^2 \theta_A = \frac{M_A^2 - M_2^2}{2M_A^2 - M_1^2 - M_2^2}, \sin^2 \theta_A = \frac{M_A^2 - M_1^2}{2M_A^2 - M_1^2 - M_2^2}. \quad (36)$$

We remind that in the formula (36) the functions $M_1^2(s)$, $M_2^2(s)$ and $B_{12}(s)$ are fixed in the point $s = M_A^2$. In the case under consideration, when the angle θ_A is a complex quantity, the values $\cos^2 \theta_A$ and $\sin^2 \theta_A$ do not determine the probability of states $|1\rangle$ and $|2\rangle$ in $|A\rangle$; indeed, the values $\sqrt{N_A} \cos \theta_A$ and $-\sqrt{N_A} \sin \theta_A$ are the transition amplitudes $|A\rangle \rightarrow |1\rangle$ and $|A\rangle \rightarrow |2\rangle$. Therefore, the corresponding probabilities are equal to $|\cos \theta_A|^2$ and $|\sin \theta_A|^2$.

In order to analyse the content of the state $|B\rangle$, an analogous expansion of the propagator matrix should be carried out near the point $s = M_B^2$. Introducing

$$|B\rangle = \sin \theta_B |1\rangle + \cos \theta_B |2\rangle, \quad (37)$$

we have the following expression for \hat{D} in the vicinity of the second pole $s = M_B^2$:

$$[\hat{D}]_{s \sim M_B^2} = \frac{N_B}{M_B^2 - s} \begin{vmatrix} \sin^2 \theta_B & \cos \theta_B \sin \theta_B \\ \sin \theta_B \cos \theta_B & \cos^2 \theta_B \end{vmatrix}, \quad (38)$$

where

$$N_B = \frac{1}{\Pi'(M_B^2)} [2M_B^2 - M_1^2 - M_2^2], \cos^2 \theta_B = \frac{M_B^2 - M_1^2}{2M_B^2 - M_1^2 - M_2^2}, \sin^2 \theta_B = \frac{M_B^2 - M_2^2}{2M_B^2 - M_1^2 - M_2^2}. \quad (39)$$

In Eqs. (38), (39) the functions $M_1^2(s)$, $M_2^2(s)$ and $B_{12}(s)$ are fixed in the point $s = M_B^2$.

If B_{12} depends on s weakly and one can neglect this dependence, the angles θ_A and θ_B coincide. In general, however, they are different. So the formulae for the propagator matrix differ from the standard approach of quantum mechanics by this very point.

Another distinction is related to the type of the level shift afforded by mixing, namely, in quantum mechanics the levels "repulse" each other from the mean value $1/2(E_1 + E_2)$ (see also Eq. (29)). Generally speaking, the equation (28) can cause both a "repulsion" of masses squared from the mean value, $1/2(M_1^2 + M_2^2)$, and an "attraction".

Let us remind now, how to write the amplitudes in the one-channel and multi-channel cases. The scattering amplitude in the one-channel case is defined by the following expression:

$$A(s) = g_i(s) D_{ij}(s) g_j(s). \quad (40)$$

In the multi-channel case, $B_{ij}(s)$ is a sum of loop diagrams: $B_{ij}(s) = \sum_a B_{ij}^{(a)}(s)$, where $B_{ij}^{(a)}$ is a loop diagram in the channel a with vertex functions $g_i^{(a)}$, $g_j^{(a)}$ and a phase space factor ρ_a . The partial scattering amplitude in the channel $a \rightarrow b$ equals

$$A_{a \rightarrow b}(s) = g_i^{(a)}(s) D_{ij}(s) g_j^{(b)}(s). \quad (41)$$

5.2.2 Construction of propagator matrix in a general case (N resonances)

Consider the construction of the propagator matrix \hat{D} for an arbitrary number (N) of resonances. The matrix elements, D_{ij} , describe the transition from the initial state i (with the bare propagator $(m_i^2 - s)^{-1}$) to the state j . They obey the system of linear equations as follows:

$$D_{ij} = D_{ik} B_{kj}(s)(m_j^2 - s)^{-1} + \delta_{ij}(m_j^2 - s)^{-1}, \quad (42)$$

where $B_{ij}(s)$ is the loop diagram for the transition $i \rightarrow j$ and δ_{ij} is the Kronecker symbol.

Let us introduce the diagonal propagator matrix \hat{d} for initial states :

$$\hat{d} = \text{diag} \left((m_1^2 - s)^{-1}, (m_2^2 - s)^{-1}, (m_3^2 - s)^{-1} \dots \right). \quad (43)$$

Then the system of linear equations (39) can be rewritten in the matrix form as

$$\hat{D} = \hat{D} \hat{B} \hat{d} + \hat{d}. \quad (44)$$

One obtains

$$\hat{D} = \frac{I}{(\hat{d}^{-1} - \hat{B})}. \quad (45)$$

The matrix \hat{d}^{-1} is diagonal, hence $\hat{D}^{-1} = (\hat{d}^{-1} - \hat{B})$ is of the form

$$\hat{D}^{-1} = \begin{vmatrix} M_1^2 - s & -B_{12}(s) & -B_{13}(s) & \dots \\ -B_{21}(s) & M_2^2 - s & -B_{23}(s) & \dots \\ -B_{31}(s) & -B_{32}(s) & M_3^2 - s & \dots \\ \vdots & \vdots & \vdots & \vdots \end{vmatrix}, \quad (46)$$

where M_i^2 is defined by Eq. (27). Inverting this matrix, we obtain a full set of elements $D_{ij}(s)$:

$$D_{ij}(s) = \frac{(-1)^{i+j} \Pi_{ji}^{(N-1)}(s)}{\Pi^{(N)}(s)}. \quad (47)$$

Here $\Pi^{(N)}(s)$ is the determinant of the matrix \hat{D}^{-1} , and $\Pi_{ji}^{(N-1)}(s)$ is a matrix supplement to the element $[\hat{D}^{-1}]_{ji}$, i.e. the matrix \hat{D}^{-1} with an excluded j -th line and i -th column.

The zeros of $\Pi^{(N)}(s)$ define the poles of the propagator matrix which correspond to physical resonances formed by the mixing. We denote the complex resonance masses as:

$$s = M_A^2, \quad M_B^2, \quad M_C^2, \dots \quad (48)$$

Near the point $s = M_A^2$, one can leave in the propagator matrix the leading pole term only. This means that the free term in Eq. (44) can be neglected, so we get a system of homogeneous equations:

$$D_{ik}(s) \left(\hat{d}^{-1} - \hat{B} \right)_{kj} = 0. \quad (49)$$

The solution of this system is defined up to the normalisation factor, and it does not depend on the initial index i . If so, the elements of the propagator matrix may be written in a factorised form as follows:

$$\left[\hat{D}^{(N)}\right]_{s \sim M_A^2} = \frac{N_A}{M_A^2 - s} \cdot \begin{vmatrix} \alpha_1^2 & \alpha_1 \alpha_2 & \alpha_1 \alpha_3 & \dots \\ \alpha_2 \alpha_1 & \alpha_2^2 & \alpha_2 \alpha_3 & \dots \\ \alpha_3 \alpha_1 & \alpha_3 \alpha_2 & \alpha_3^2 & \dots \\ \dots & \dots & \dots & \dots \end{vmatrix}, \quad (50)$$

where N_A is the normalisation factor chosen to satisfy the condition

$$\alpha_1^2 + \alpha_2^2 + \alpha_3^2 + \dots + \alpha_N^2 = 1. \quad (51)$$

The constants α_i are the normalised amplitudes for the *resonance* $A \rightarrow \text{state } i$ transitions. The probability to find the state i in the physical resonance A is equal to:

$$w_i = |\alpha_i|^2. \quad (52)$$

Analogous representations of the propagator matrix can be given also in the vicinity of other poles:

$$D_{ij}^{(N)}(s \sim M_B^2) = N_B \frac{\beta_i \beta_j}{M_B^2 - s}, \quad D_{ij}^{(N)}(s \sim M_C^2) = N_C \frac{\gamma_i \gamma_j}{M_C^2 - s} \quad \dots \quad (53)$$

The coupling constants satisfy normalisation conditions similar to that of Eq. (48):

$$\beta_1^2 + \beta_2^2 + \dots + \beta_N^2 = 1, \quad \gamma_1^2 + \gamma_2^2 + \dots + \gamma_N^2 = 1, \quad \dots \quad (54)$$

In the general case, however, there is no completeness condition for the inverse expansion:

$$\alpha_i^2 + \beta_i^2 + \gamma_i^2 + \dots \neq 1. \quad (55)$$

For two resonances this means that $\cos^2 \Theta_A + \sin^2 \Theta_B \neq 1$. Still, let us remind that the equality in the inverse expansion, which is relevant for the completeness condition, appears in models where the s -dependence of the loop diagrams is neglected.

5.2.3 Full resonance overlapping: the accumulation of widths of neighbouring resonances by one of them

Let us consider two examples which describe the idealised situation of a full overlapping of two or three resonances. In these examples, the effect of accumulation of widths of neighbouring resonances by one of them can be seen in its original untouched form.

a) *Full overlapping of two resonances.*

For the sake of simplicity, let B_{ij} be a weak s -dependent function; Eq. (29) may be used. We define:

$$M_1^2 = M_R^2 - iM_R\Gamma_1, \quad M_2^2 = M_R^2 - iM_R\Gamma_2, \quad (56)$$

and put

$$\text{Re} B_{12}(M_R^2) = P \int_{(\mu_1 + \mu_2)^2}^{\infty} \frac{ds' g_1(s') g_2(s') \rho(s')}{\pi (s' - M_R^2)} \rightarrow 0. \quad (57)$$

It is possible that $\text{Re}B_{12}(M_R^2)$ equals zero at positive g_1 and g_2 , if the contribution from the integration region $s' < M_R^2$ cancels the contribution from the $s' > M_R^2$ region. In this case

$$B_{12}(M_R^2) \rightarrow ig_1(M_R^2)g_2(M_R^2)\rho(M_R^2) = iM_R\sqrt{\Gamma_1\Gamma_2}. \quad (58)$$

Substituting Eqs. (53)–(55) into Eq. (45), one has:

$$M_A^2 \rightarrow M_R^2 - iM_R(\Gamma_1 + \Gamma_2) \quad M_B^2 \rightarrow M_R^2. \quad (59)$$

Therefore, after mixing, one of the states accumulates the widths of primary resonances, $\Gamma_A \rightarrow \Gamma_1 + \Gamma_2$, and another state becomes a quasi-stable particle, with $\Gamma_B \rightarrow 0$.

b) *Full overlapping of three resonances.*

Consider the equation

$$\Pi^{(3)}(s) = 0 \quad (60)$$

in the same approximation as in the above example. Correspondingly, we put:

$$\text{Re}B_{ab}(M_R^2) \rightarrow 0, (a \neq b); \quad M_i^2 = M_R^2 - s - iM_R\Gamma_i = x - i\gamma_i. \quad (61)$$

A new variable, $x = M_R^2 - s$, is used, and we denote $M_R\Gamma_i = \gamma_i$. Taking into account $B_{ij}B_{ji} = -\gamma_i\gamma_j$ and $B_{12}B_{23}B_{31} = -i\gamma_1\gamma_2\gamma_3$, we can rewrite the equation (60) as follows:

$$x^3 + x^2(i\gamma_1 + i\gamma_2 + i\gamma_3) = 0. \quad (62)$$

Therefore, at full resonance overlapping, one obtains:

$$M_A^2 \rightarrow M_R^2 - iM_R(\Gamma_1 + \Gamma_2 + \Gamma_3), \quad M_B^2 \rightarrow M_R^2, \quad M_C^2 \rightarrow M_R^2. \quad (63)$$

Thus, the resonance A has accumulated the widths of three primary resonances, and the states B and C became quasi-stable and degenerate.

6 The $q\bar{q}$ - gg content of f_2 -mesons, observed in the reactions $p\bar{p} \rightarrow \pi^0\pi^0, \eta\eta, \eta\eta'$

We determine here the $q\bar{q}$ - gg content of f_2 -mesons, observed in the reactions $p\bar{p} \rightarrow \pi^0\pi^0, \eta\eta, \eta\eta'$ [2]. This determination is based on experimentally observed relations (3) and the rules of quark combinatorics taken into account in the leading terms of the $1/N$ -expansion.

For the $f_2 \rightarrow \pi^0\pi^0, \eta\eta, \eta\eta'$ transitions, when the $q\bar{q}$ -meson is a mixture of quarkonium and gluonium components, the decay vertices read in the leading terms of the $1/N$ -expansion (see Tables 3 and 4) as follows:

$$\begin{aligned} g_{\pi^0\pi^0}^{q\bar{q}-meson} &= g \frac{\cos\varphi}{\sqrt{2}} + \frac{G}{\sqrt{2+\lambda}}, \\ g_{\eta\eta}^{q\bar{q}-meson} &= g \left(\cos^2\theta \frac{\cos\varphi}{\sqrt{2}} + \sin^2\theta \sqrt{\lambda} \sin\varphi \right) + \frac{G}{\sqrt{2+\lambda}} (\cos^2\theta + \lambda \sin^2\theta), \\ g_{\eta\eta'}^{q\bar{q}-meson} &= \sin\theta \cos\theta \left[g \left(\frac{\cos\varphi}{\sqrt{2}} - \sqrt{\lambda} \sin\varphi \right) + \frac{G}{\sqrt{2+\lambda}} (1-\lambda) \right]. \end{aligned} \quad (64)$$

The terms proportional to g stand for the $q\bar{q} \rightarrow \text{two mesons}$ transitions ($g = g^L \cos \alpha$), while the terms with G represent the $\text{gluonium} \rightarrow \text{two mesons}$ transition ($G = G^L \sin \alpha$). Consequently, G^2 and g^2 are proportional to the probabilities for finding gluonium ($W = \sin^2 \alpha$) and quarkonium ($1 - W$) components in the considered f_2 -meson. Let us remind that the mixing angle Θ stands for the $n\bar{n}$ and $s\bar{s}$ components in the η and η' mesons; we neglect the possible admixture of a gluonium component to η and η' (according to [47], the gluonium admixture to η is less than 5%, to η' — less than 20%). For the mixing angle Θ we take $\Theta = 37^\circ$.

6.1 The analysis of the quarkonium-gluonium contents of the $f_2(1920)$, $f_2(2020)$, $f_2(2240)$, $f_2(2300)$

Making use of the data (3), the relations (64) allow us to find φ as a function of the ratio G/g of the coupling constants. The result for the resonances $f_2(1920)$, $f_2(2020)$, $f_2(2240)$, $f_2(2300)$ is shown in Fig. 17. Solid curves enclose the values of $g_{\eta\eta}/g_{\pi^0\pi^0}$ for $\lambda = 0.6$ (this is the $\eta\eta$ -zone in the $(G/g, \varphi)$ plane) and dashed curves enclose $g_{\eta\eta'}/g_{\pi^0\pi^0}$ for $\lambda = 0.6$ (the $\eta\eta'$ -zone). The values of G/g and φ , lying in both zones, describe the experimental data (3): these regions are shadowed in Fig. 17.

The correlation curves in Fig. 17 enable us to give a qualitative estimate for the change of the angle φ (i.e. the relation of the $n\bar{n}$ and $s\bar{s}$ components in the f_2 meson) depending on the value of the gluonium admixture. The values g^2 and G^2 are proportional to the probabilities of having quarkonium and gluonium components in the f_2 meson, $g^2 = (g^L)^2(1 - W)$ and $G^2 = (G^L)^2W$. Here W is the probability of a gluonium admixture in the considered $q\bar{q}$ -meson; g^L and G^L are universal constants, see Tables 3 and 4. Since $G^L/g^L \sim 1/\sqrt{N_c}$ and $W \sim 1/N_c$, we can give a rough estimate:

$$\frac{G^2}{g^2} \sim \frac{W}{N_c(1 - W)} \rightarrow \frac{W}{10}. \quad (65)$$

Let us remind that the numerical calculations of the diagrams indicate that $1/N_c$ leads to a smallness of the order of $1/10$ — this is taken into account in (65). Assuming that the gluonium components are less than 20% ($W < 0.2$) in each of the $q\bar{q}$ resonances $f_2(1920)$, $f_2(2020)$, $f_2(2240)$, $f_2(2300)$, we put roughly $W \simeq 10 G^2/g^2$, and obtain for the angles φ the following intervals:

$$\begin{aligned} W_{\text{gluonium}}[f_2(1920)] < 20\% : \quad & -0.8^\circ < \varphi[f_2(1920)] < 3.6^\circ, \\ W_{\text{gluonium}}[f_2(2020)] < 20\% : \quad & -7.5^\circ < \varphi[f_2(2020)] < 13.2^\circ, \\ W_{\text{gluonium}}[f_2(2240)] < 20\% : \quad & -8.3^\circ < \varphi[f_2(2240)] < 17.3^\circ, \\ W_{\text{gluonium}}[f_2(2300)] < 20\% : \quad & -25.6^\circ < \varphi[f_2(2300)] < 9.3^\circ \end{aligned} \quad (66)$$

6.2 The $n\bar{n}$ - $s\bar{s}$ content of the $q\bar{q}$ -mesons

Let us summarise what we know about the status of the ($I = 0, J^{PC} = 2^{++}$) $q\bar{q}$ -mesons. Estimating the $n\bar{n}$ - $s\bar{s}$ content of the f_2 -mesons, we ignore the gg admixture (remembering that

it is of the order of $\sin^2 \alpha \sim 1/N_c$.

1. The resonances $f_2(1270)$ and $f'_2(1525)$ are well-known partners of the basic nonet with $n = 1$ and a dominant P -component, $1^3P_2 q\bar{q}$. Their flavour content, obtained from the reaction $\gamma\gamma \rightarrow K_S K_S$, is

$$\begin{aligned} f_2(1270) &= \cos \varphi_{n=1} n\bar{n} + \sin \varphi_{n=1} s\bar{s}, \\ f_2(1525) &= -\sin \varphi_{n=1} n\bar{n} + \cos \varphi_{n=1} s\bar{s}, \\ \varphi_{n=1} &= -1 \pm 3^\circ. \end{aligned} \tag{67}$$

2. The resonances $f_2(1560)$ and $f_2(1750)$ are partners in a nonet with $n = 2$ and a dominant P -component, $2^3P_2 q\bar{q}$. Their flavour content, obtained from the reaction $\gamma\gamma \rightarrow K_S K_S$, is

$$\begin{aligned} f_2(1560) &= \cos \varphi_{n=2} n\bar{n} + \sin \varphi_{n=2} s\bar{s}, \\ f_2(1750) &= -\sin \varphi_{n=2} n\bar{n} + \cos \varphi_{n=2} s\bar{s}, \\ \varphi_{n=2} &= -10^{+5}_{-10}^\circ. \end{aligned} \tag{68}$$

3. The resonances $f_2(1920)$ and $f_2(2120)$ [4] (in [1] they are denoted as $f_2(1910)$ and $f_2(2010)$) are partners in a nonet with $n = 3$ and with a dominant P -component, $3^3P_2 q\bar{q}$. Ignoring the contribution of the glueball component, their flavour content, obtained from the reactions $p\bar{p} \rightarrow \pi^0 \pi^0, \eta\eta, \eta\eta'$, is

$$\begin{aligned} f_2(1920) &= \cos \varphi_{n=3} n\bar{n} + \sin \varphi_{n=3} s\bar{s}, \\ f_2(2120) &= -\sin \varphi_{n=3} n\bar{n} + \cos \varphi_{n=3} s\bar{s}, \\ \varphi_{n=3} &= 0 \pm 5^\circ. \end{aligned} \tag{69}$$

4. The next, predominantly 3P_2 states with $n = 4$ are $f_2(2240)$ and $f_2(2410)$ [4]. (By mistake, in [1] the resonance $f_2(2240)$ [2] is listed as $f_2(2300)$, while $f_2(2410)$ [4] is denoted as $f_2(2340)$). Their flavour content at $W = 0$ is determined as

$$\begin{aligned} f_2(2240) &= \cos \varphi_{n=4} n\bar{n} + \sin \varphi_{n=4} s\bar{s}, \\ f_2(2410) &= -\sin \varphi_{n=4} n\bar{n} + \cos \varphi_{n=4} s\bar{s}, \\ \varphi_{n=4} &= 5 \pm 11^\circ. \end{aligned} \tag{70}$$

5. $f_2(2020)$ and $f_2(2340)$ [4] belong to the basic F -wave nonet ($n = 1$) (in [1] the $f_2(2020)$ [2] is denoted as $f_2(2000)$ and is put in the section "Other light mesons", while $f_2(2340)$ [4] is denoted as $f_2(2300)$). The flavour content of the 1^3F_2 mesons is

$$\begin{aligned}
f_2(2020) &= \cos \varphi_{n(F)=1} n\bar{n} + \sin \varphi_{n(F)=1} s\bar{s}, \\
f_2(2340) &= -\sin \varphi_{n(F)=1} n\bar{n} + \cos \varphi_{n(F)=1} s\bar{s}, \\
\varphi_{n(F)=1} &= 5 \pm 8^\circ.
\end{aligned} \tag{71}$$

6. The resonance $f_2(2300)$ [2] has a dominant F -wave quark-antiquark component; its flavour content for $W = 0$ is defined as

$$f_2(2300) = \cos \varphi_{n(F)=2} n\bar{n} + \sin \varphi_{n(F)=2} s\bar{s}, \quad \varphi_{n(F)=2} = -8^\circ \pm 12^\circ. \tag{72}$$

A partner of $f_2(2300)$ in the 2^3F_2 nonet has to be a f_2 -resonance with a mass $M \simeq 2570$ MeV.

7 Conclusion

The broad $f_2(2000)$ state is the descendant of the lowest tensor glueball. This statement is favoured by estimates of parameters of the Pomeron trajectory (e.g., see [5], Chapter 5.4, and references therein), according to which $M_{2^{++}glueball} \simeq 1.7 - 2.5$ GeV. Lattice calculations result in a similar value, namely, 2.2–2.4 GeV [21]. The corresponding coupling constants $f_2(2000) \rightarrow \pi^0\pi^0, \eta\eta, \eta\eta'$ satisfy the relations for the glueball, eq.(22), with $\lambda \simeq 0.5 - 0.7$. The admixture of the quarkonium component $(q\bar{q})_{glueball}$ in $f_2(2000)$ cannot be determined by the ratios of the coupling constants between the hadronic channels; to define it, $f_2(2000)$ has to be observed in $\gamma\gamma$ -collisions. The value of $(q\bar{q})_{glueball}$ in $f_2(2000)$ may be rather large: the rules of $1/N$ -expansion give a value of the order of N_f/N_c . It is, probably, just the largeness of the quark-antiquark component in $f_2(2000)$ which results in its suppressed production in the radiative J/ψ decays (see discussion in [8]).

We have now two observed glueballs, a scalar $f_0(1200 - 1600)$ [14, 15] (see also [5, 12]) and a tensor one, $f_2(2000)$. It is illustrative to present the situation with $0^{++}, 2^{++}$ glueballs on the (J, M^2) -plane, we demonstrate this in Fig. 18. According to various estimates, the leading Pomeron trajectory has an intercept at $\alpha(0) \simeq 1.10 - 1.30$ (see, for example, [18, 19, 20]). Assuming that the Pomeron trajectory has a linear behaviour, which does not contradict experimental data, $\alpha_P(M^2) = \alpha_P(0) + \alpha'_P(0)M^2$, we have for the slope $\alpha'_P(0) = 0.20 \pm 0.05$. The scalar glueball $f_0(1200 - 1600)$ is located on the daughter trajectory which predicts the second tensor glueball at $M \simeq 3.45$ GeV. If the Pomeron trajectories in (n, M^2) plane are linear, similar to the $q\bar{q}$ -trajectories, then the next scalar glueball (radial excitation of gg gluonium) should be at $M \simeq 3.2$ GeV.

Observed glueball states have transformed into broad resonances owing to the accumulation of widths of their neighbours. The existence of a low-lying pseudoscalar glueball is also expected. It is natural to assume that it has also transformed into a broad resonance. Consequently, the question is, where to look for this broad 0^{-+} state. There are two regions in which we can

suspect the existence of a pseudoscalar glueball: in the region of 1700 MeV or much higher, at ~ 2300 MeV, see the discussion in [8] (Section 10.5). In [50] it is suggested that the lowest scalar and pseudoscalar glueballs must have roughly equal masses. If so, a 0^{-+} glueball has to occur in the 1700 MeV region.

The authors are grateful to D.V. Bugg, L.D. Faddeev and S.S. Gershtein for stimulating discussions. The paper was supported by the grant No. 04-02-17091 of the RFFI.

References

- [1] S. Eidelman *et al.* (PDG), Phys. Lett. B **592**, 1 (2004).
- [2] A.V. Anisovich *et al.*, Phys. Lett. B **491**, 47 (2000).
- [3] D. Barberis *et al.* (WA 102 Collab.), Phys. Lett. B **471**, 440 (2000).
- [4] R.S. Longacre and S.J. Lindenbaum, Report BNL-72371-2004.
- [5] V.V. Anisovich, M.N. Kobrinsky, J. Nyiri, Yu.M. Shabelski, "*Quark model and high energy collisions*", second edition, World Scientific, 2004.
- [6] V.A. Schegelsky, A.V. Sarantsev, V.A. Nikonov, "Phenomenological investigation of the $K_S K_S$ final state in two-photon collisions and nonet classification of tensor resonances", L3 Note 3001, October 27, 2004.
- [7] A. Etkin *et al.*, Phys. Lett. B **165**, 217 (1985); B **201**, 568 (1988).
- [8] D.V. Bugg, Phys. Rep., **397**, 257 (2004).
- [9] V.V. Anisovich, Pis'ma v ZhETF, **80**, 845 (2004) [JETP Letters, **80**, 715 (2004)].
- [10] V.A. Schegelsky and A.V. Sarantsev, *Resonances in $\gamma\gamma \rightarrow 3\pi$ reaction*, Talk given at XXXIX PNPI Winter School (2005).
- [11] A.V. Anisovich, V.V. Anisovich and A.V. Sarantsev, Phys. Rev. D **62**, 051502 (2000).
- [12] V.V. Anisovich, UFN, **174**, 49 (2004) [Physics-Uspekhi, **47**, 45 (2004)].
- [13] V.V. Anisovich, D.V. Bugg and A.V. Sarantsev, Phys. Rev. D **58**, 111503 (1998).
- [14] V.V. Anisovich, Yu.D. Prokoshkin and A.V. Sarantsev, Phys. Lett. B **389**, 388 (1996); Z. Phys. A **357**, 123 (1997).
- [15] A.V. Anisovich, V.V. Anisovich and A.V. Sarantsev, Phys. Lett. B **395**, 123 (1997); Z. Phys. A **359**, 173 (1997).
- [16] V.V. Anisovich, M.A. Matveev, J. Nyiri and A.V. Sarantsev, Yad. Fiz., in press hep-ph/0501003.
- [17] V.V. Anisovich and A.V. Sarantsev, Pis'ma v ZhETF, **81**, 531 (2005), [JETP Letters, **81**, 417 (2005)].
- [18] A.B. Kaidalov and K.A. Ter-Martirosyan, Sov. J. Nucl. Phys. **39**, 979 (1984).
- [19] P.V. Landshoff, "Soft hadron reactions", in *QCD: 20 Years Later*, eds. P.M. Zerwas and H.A. Kastrup, (World Scientific, Singapore, 1993).
- [20] L.G. Dakhno and V.A. Nikonov, Eur. Phys. J. A **5**, 209 (1999).

- [21] G.S. Bali, K. Schilling, A. Hulsebos et al. (UK QCD Collab.), Phys. Lett. B **309**, 378 (1993);
C.J. Morningstar, M.J. Peardon, Phys. Rev. D **60**, 034509
M. Loan, X-Q. Luo and Z-H.Luo, hep-lat/0503038. (1999).
- [22] U. Loering, B.C. Metsch and H.R. Petry, Eur. Phys. J. A**10**, 447 (2001).
- [23] E. Klempt, Eur.Phys.J. C**28** (2003), hep-ex/0206012.
- [24] D.V. Bugg and A.V. Sarantsev, B.S. Zou, Nucl. Phys. B**471**, 59 (1996).
- [25] G. Grayer et al., Nucl. Phys. B**75**, 189 (1974).
- [26] V.V. Anisovich and A.V. Sarantsev, Eur. Phys. J. A **16**, 229 (2003).
- [27] D.V. Amelin et al. (VES Collab.), Z. Phys. C**70**, 71 (1996).
- [28] V.V. Anisovich, D.I. Melikhov, V.A. Nikonov, Phys. Rev. D **55**, 2918 (1997).
- [29] A.V. Anisovich, V.V. Anisovich and V.A. Nikonov, Eur. Phys. J. A**12**, 103 (2001);
A.V. Anisovich, V.V. Anisovich, M.A. Matveev and V.A. Nikonov, Yad. Fiz. **66**, 946 (2003)
[Phys. Atom. Nucl. **66**, 914 (2003)].
- [30] A.V. Anisovich, V.V. Anisovich, L.G. Dakhno, V.A. Nikonov and A.V. Sarantsev, Yad. Fiz., in press, hep-ph/0406320.
- [31] J.Z. Bai et al., Phys. Rev. D**68**, 052003 (2003); Phys. Lett. B **472**, 207 (2000).
- [32] V.V. Anisovich, UFN, **168**, 481 (1998) [Physics-Uspekhi, **41**, 419 (1998)].
- [33] G. 't Hooft, Nucl. Phys. B **72**, 461 (1974).
- [34] G. Veneziano, Nucl. Phys. B **117**, 519 (1976).
- [35] F.E. Close and A. Kirk, Eur. Phys. J. C**21**, 531 (2001).
- [36] W. Lee and D. Weingarten, Phys. Rev. D**60**, 034509 (1999).
- [37] I.S. Shapiro, Nucl. Phys. A **122** 645 (1968).
- [38] I.Yu. Kobzarev, N.N. Nikolaev, L.B. Okun, Yad. Fiz. **10**, 864 (1969); [Sov. J. Nucl. Phys. **10**, 499 (1960)].
- [39] L. Stodolsky, Phys. Rev. D **1**, 2683 (1970).
- [40] A.V. Anisovich, V.A. Nikonov, A.V. Sarantsev, V.V. Sarantsev, in "PNPI XXX, *Scientific Highlight, Theoretical Physics Division*, Gatchina (2001), p. 58.(1999).
- [41] S.M. Flatté, Phys. Lett. **B63**, 224 (1976).

- [42] E. Eisenhandler et al., Nucl. Phys. B**98**, 109 (1975);
A. Hasan et al., Nucl. Phys. B**378**, 3 (1992).
- [43] A.V. Anisovich, hep-ph/0104005.
- [44] V.V. Anisovich, M.G. Huber, M.N. Kobrinsky and B.Ch. Metsch, Phys. Rev. D **42**, 3045 (1990);
V.V. Anisovich, V.A. Nikonov and J. Nyiri, Yad. Fiz. **64**, 1 (2001).
- [45] K. Peters, E. Klempt, Phys. Lett. B **352**, 467 (1995).
- [46] S.S. Gershtein, A.K. Likhoded, Yu.D. Prokoshkin, Z. Phys. C **24**, 305 (1984);
C. Amsler, F.E. Close, Phys. Rev. D **53**, 295 (1996); Phys. Lett. B **353**, 385 (1995);
V.V. Anisovich, Phys. Lett. B **364**, 195 (1995).
- [47] V.V. Anisovich, D.V. Bugg, D.I. Melikhov, V.A. Nikonov, Phys. Lett. B **404**, 166 (1997).
- [48] A.A. Carter et al., Phys. Lett. B **67**, 117 (1977).
- [49] A.V. Anisovich, V.V. Anisovich, V.N. Markov, M.A. Matveev and A.V. Sarantsev, J. Phys. G: Nucl. Part. Phys. **28**, 15 (2002).
- [50] L. Faddeev, A.J. Niemi and U. Wiedner, hep-ph/0308240 (2003).
- [51] A.V. Anisovich *et al.*, Phys. Lett. B **452**, 173 (1999); Phys. Lett. B **452**, 187 (1999); Phys. Lett. B **517**, 261 (2001);

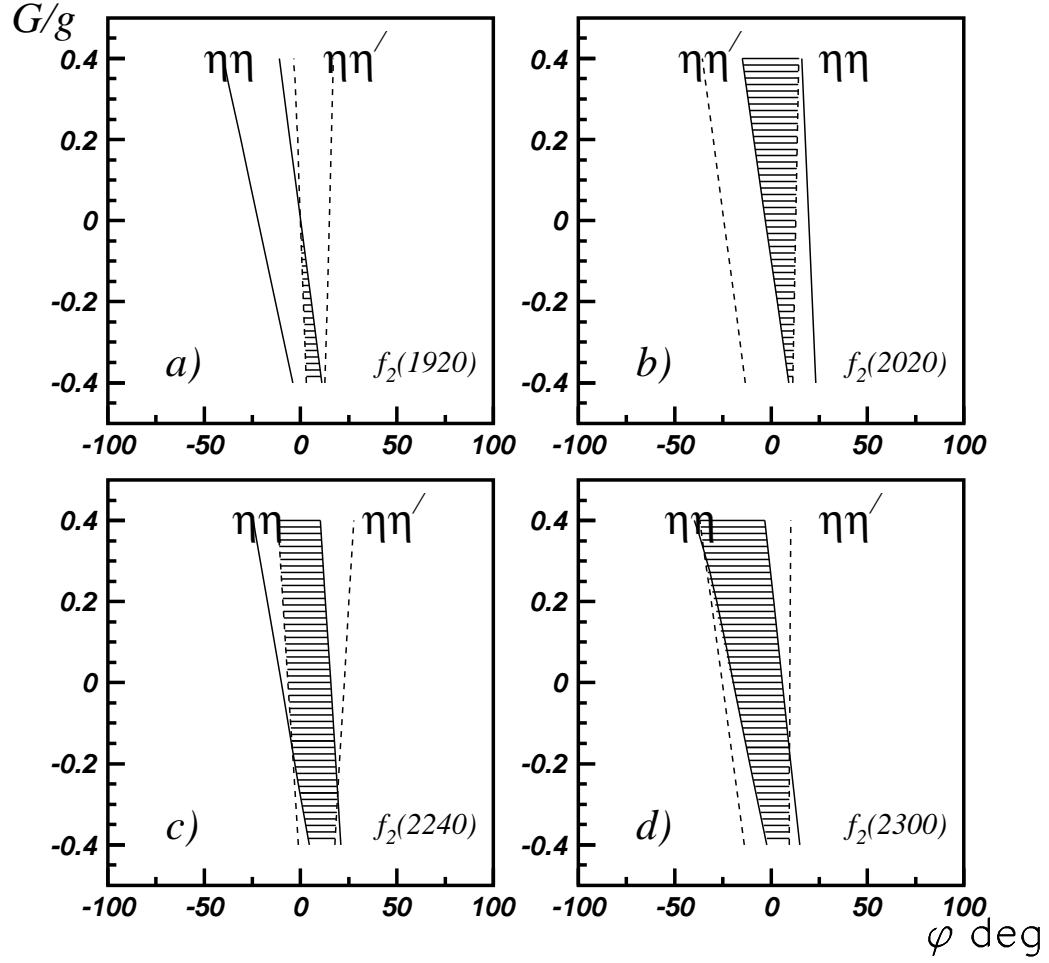


Figure 17: Correlation curves $g_{\eta\eta}(\varphi, G/g)/g_{\pi^0\pi^0}(\varphi, G/g)$ and $g_{\eta\eta'}(\varphi, G/g)/g_{\pi^0\pi^0}(\varphi, G/g)$ drawn according to (64) at $\lambda = 0.6$ for $f_2(1920)$, $f_2(2020)$, $f_2(2240)$, $f_2(2300)$ [2,17]. Solid and dashed curves enclose the values $g_{\eta\eta}(\varphi, G/g)/g_{\pi^0\pi^0}(\varphi, G/g)$ and $g_{\eta\eta'}(\varphi, G/g)/g_{\pi^0\pi^0}(\varphi, G/g)$ which obey (3) (the zones $\eta\eta$ and $\eta\eta'$ in the $(G/g, \varphi)$ plane). The values of G/g and φ , lying in both zones describe the experimental data (3): these are the shadowed regions.

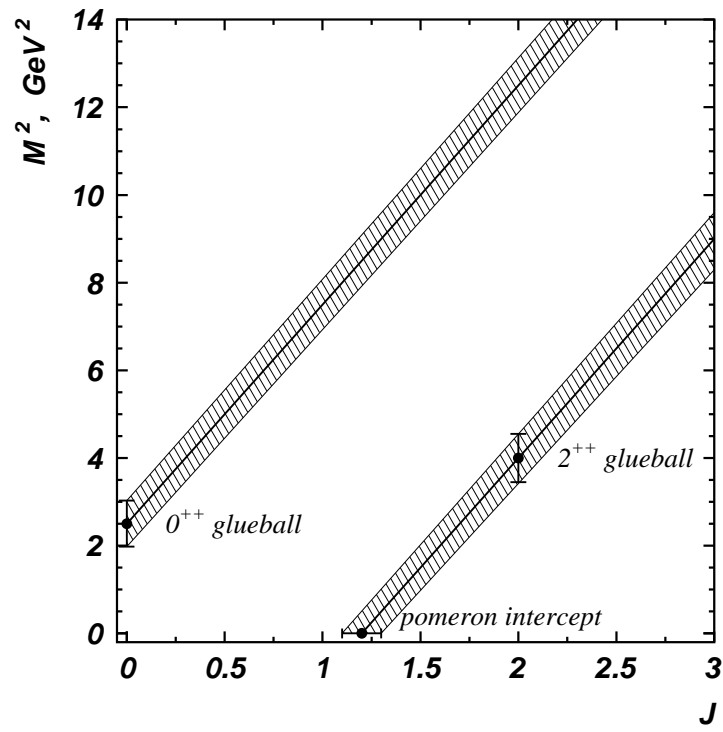


Figure 18: Glueball states on the Pomeron trajectories.